J. Fluid Mech. (2011), *vol.* 680, *pp.* 534–563.
doi:10.1017/jfm.2011.186

Large-scale motions and inner/outer layer interactions in turbulent Couette–Poiseuille flows

SERGIO PIROZZOLI†, MATTEO BERNARDINI AND PAOLO ORLANDI

Dipartimento di Meccanica e Aeronautica, Università di Roma 'La Sapienza', Via Eudossiana 18, 00184 Roma, Italy

(Received 28 October 2010; revised 12 April 2011; accepted 14 April 2011; first published online 31 May 2011)

We investigate the organization of the momentum-carrying eddies in turbulent Couette–Poiseuille flows. The study relies on a direct numerical simulation (DNS) database covering a wide range of flow configurations from pure Couette to pure Poiseuille flows, at $Re_\tau \approx 250$ (based on the flow properties at the stationary wall). The study highlights the occurrence of streaky patterns of alternating high and low momentum throughout the channel for all flow configurations, except near zeros of the mean shear, where streaks are suppressed. The mean streak spacing shows a relatively universal distribution in the core of the channel, where it ranges from 50 to 100 local viscous units. The validity of the local viscous scaling in collapsing flow features at different wall distances is confirmed by the analysis of the spanwise velocity spectra, which also highlights (in the case of Couette-like flows) the onset of a secondary low-wavenumber flow mode, superposed on the high-wavenumber flow mode that is responsible for the inner-layer dynamics. The effect of the former mode on the latter is studied by means of the two-point amplitude modulation coefficient, which brings to light a nonlinear modulation phenomenon. Physical mechanisms to explain the modulation effect are proposed, based on the interpretation of the conditional average events. Note that, although similar mechanisms have been previously observed in high-Reynolds-number turbulent boundary layers and channels, the modulation effect is here rather associated with the intrinsic large-scale dynamics of Couette-like flows, and takes place at DNS-accessible Reynolds numbers. We thus believe that the study of Couette-like flows may give an alternative avenue for probing inner/outer interaction effects than canonical channel flows.

Key words: boundary layer structure, shear layer turbulence, turbulence simulation

1. Introduction

The near-wall region of turbulent flows has been extensively investigated in boundary layers, channels and pipes. Experiments and direct numerical simulations (DNS) performed in a wide range of Reynolds numbers have established the existence of coherent structures populating the inner layer of wall-bounded flows, which are primarily responsible for sustaining the turbulence. As shown by early experimental works (Wallace, Eckelmann & Brodkey 1972; Willmarth & Lu 1972), a large fraction of turbulence kinetic energy in wall-bounded flows is produced in the buffer layer

† Email address for correspondence: sergio.pirozzoli@uniroma1.it

during bursting processes, consisting of violent outward ejections of low-speed fluid that is pumped up and away from the wall, and sweeps of high-speed fluid towards the wall. As a consequence, the near-wall velocity field is organized into narrow regions of alternating low and high momentum, referred to as streaks, being the signature of ejection and sweep events, respectively. Streaks have a characteristic length of about 100 wall units in the spanwise direction (Kline *et al.* 1967) and are associated with the occurrence of counter-rotating vortex pairs aligned in the streamwise direction (Robinson 1991). Streaks and quasi-streamwise vortices are currently regarded to be the elementary units responsible for the regeneration cycle of near-wall turbulence (Hamilton, Kim & Waleffe 1995; Schoppa & Hussain 2002), whereby quasi-streamwise vortices act on the mean shear to create the streaks, which become inviscidly unstable and eventually produce tilted streamwise vortices. An alternative vortex regeneration mechanism, which does not explicitly involve the streaks, was proposed by Orlandi & Jiménez (1994), based on the idea that when a vortex approaches a no-slip wall, it induces a layer of vorticity of opposite sign, which may roll up into new vortices. The new vorticity, which is already predominantly streamwise, leaves the wall under the induction of its parent, and is stretched and intensified by the mean shear. The interaction generates local wall-normal velocities and may directly lead to the formation of new streaks. Following Jiménez & Pinelli (1999), these two mechanisms will hereafter be referred to as the 'streaks cycle' and the 'wall cycle', respectively.

While it is believed that the streaks/streamwise vortices pattern is a universal feature of wall-bounded flows, much less is known about the organization of turbulence away from walls. It is a relatively recent finding that the outer part of boundary layers, as well as the core region of channels and pipes, is characterized by large coherent structures, having the same qualitative features as the near-wall streaks, i.e. an alternating pattern of low- and high-speed momentum, but scaling in outer flow units (i.e. either the boundary-layer thickness, the channel height or the pipe radius). From inspection of the pre-multiplied energy spectra of streamwise velocity fluctuations, Kim & Adrian (1999) first identified very-large-scale motions (VLSM) in pipe flow, having a typical length of up to 14 pipe radii. Hutchins & Marusic (2007) observed the occurrence of elongated regions of positive and negative momentum fluctuations in the logarithmic region of turbulent boundary layers, extending for at least six boundary-layer thicknesses, that they called superstructures or large-scale motions (LSM). Large-scale and very-large-scale motions in wall-bounded flows have been addressed in detail in the recent studies by Monty *et al.* (2007) and Mathis *et al.* (2009*b*). It has been found that large-scale motions in the outer layer superpose onto the near-wall turbulence, causing deviations from the universal wall scaling at sufficiently large Reynolds number. Such an effect mainly manifests itself as a slow (logarithmic) increase of the streamwise turbulence intensity (Hoyas & Jiménez 2006). Large-scale motions are also responsible for more subtle phenomena of amplitude modulation of the near-wall coherent structures, whereby (Mathis, Hutchins & Marusic 2009*a*) positive large-scale velocity fluctuations above the wall cause increased small-scale near-wall turbulent activity. As observed by Morrison (2007), mechanisms of amplitude modulation are inherently nonlinear, and cannot be simply traced back to the imprint of superstructures on the near-wall region. For LSM and VLSM to be energetically significant and affect the inner-layer dynamics, clear separation between inner and outer turbulence scales is necessary, which implies high Reynolds numbers. Therefore, inner/outer layer interactions have mostly been observed in experiments, and remain (so far) inaccessible for most DNS, except for

some recent remarkable efforts (Hoyas & Jiménez 2006; Schlatter *et al.* 2009; Jiménez *et al.* 2010).

It is important to note that streaks are not an exclusive feature of wall-bounded flows, and the presence of a solid boundary is indeed not strictly necessary. Lee, Kim & Moin (1990) showed that homogeneous turbulence subjected to intense shear exhibits coherent flow patterns which closely resemble the streaks found in the near-wall region of wall-bounded flows. They noted that the formation of streaky structures is primarily controlled by the value of a dimensionless shear parameter $\sigma k/\varepsilon$ (where σ is the mean shear, k is the turbulence kinetic energy, and ε is its dissipation rate), which is a measure of the ratio between the eddy turnover time k/ε and the time scale of mean deformation $1/\sigma$. Lam & Banerjee (1992) arrived at similar conclusions, but identified the production-to-dissipation ratio $\sigma|\overline{u'v'}|/\varepsilon$ as the controlling parameter for the occurrence of streaks.

The class of the Couette–Poiseuille flows (hereafter C–P) allows introduction of an additional degree of freedom in the study of channel flows, and in particular to establish the effect of the movement of one of the two walls. As will be shown later, this special feature makes C–P flows a good candidate for study of the interaction of the large-scale structures in the channel core with the near-wall turbulence. Besides their intrinsic theoretical interest, C–P flows have also been used as a basis for analysing the resilience of the logarithmic law to pressure gradients (Johnstone, Coleman & Spalart 2010), and for understanding the mechanisms of drag reduction in ultra-hydrophobic surfaces (Spencer *et al.* 2009), which can be regarded as surfaces having a finite slip velocity.

An experimental apparatus for the study of C–P flows was first designed by El Telbany & Reynolds (1980, 1981), who performed extensive measurements of mean and fluctuating velocities. Those early studies highlighted difficulties in achieving universal scaling of the velocity fluctuations, especially near the moving wall, and the moderate success of scaling based on the local value of the total shear stress in collapsing data in the core of the channel. Thurlow & Klewicki (2000) found evidence for exchange of fluid momentum between the two walls, which is increased when one of the walls is put into motion, and disturbances originating from the stationary wall may impinge onto the moving wall. Nakabayashi, Kitoh & Katoh (2004) investigated the similarity laws of the mean velocity profiles and the influence of mean shear and Reynolds number, and argued about the different structure of Poiseuille-like flows, for which the mean shear vanishes at a point in the channel, and Couette-like flows, for which the mean shear never vanishes, and which exhibit a global circulatory motion. Those observations were made more precise by Kitoh, Nakabayashi & Nishimura (2005), who focused on the extreme case of the Couette flow, and inferred the existence of large longitudinal vortices in the central part of the channel. For this reason, Couette flow has characteristic length scales that are much longer than those found in Poiseuille flow.

DNS gives access to all flow properties of interest, thus bypassing the inherent limitations of experimental investigations. In particular, DNS allows a detailed analysis of the near-wall region, where most turbulence production takes place. The limiting case of Poiseuille flow has of course been extensively analysed over the years (see Hoyas & Jiménez 2006 for some recent developments). The other limiting case of Couette flow has comparatively received much less attention, one of the most relevant studies being Bech *et al.* (1995). They performed DNS at low Reynolds number (the friction Reynolds number was $Re_\tau = 82$) and carried out a conditional eduction of coherent structures in the near-wall region based on the variable interval

time averaging (VITA) technique. The study showed a similar pattern of the near-wall turbulence compared to canonical Poiseuille flow, which is dominated by meandering streaks and shear layers. However, an extension of the near-wall correlations into the channel core was observed, which led the authors to infer a closer influence of the outer region in the case of Couette flow. In DNS at $Re_\tau = 52$ in a very large domain, Komminaho, Lundbladh & Johansson (1996) found that the typical large-scale structures developing in the inner part of the channel have a spanwise separation of about $4h$ and a length of about $30h$. To our knowledge, the only extensive DNS study of C–P flows (although limited to Poiseuille-like flow conditions) was performed by Kuroda, Kasagi & Hirata (1993). They considered low-Reynolds-number flows (at $Re_\tau \approx 150$) and reported velocity statistics and Reynolds stress budgets. Based on the analysis of instantaneous flow visualizations, they concluded that the mean shear rate plays a primary role in the mechanisms of generation of coherent structures near the wall.

In the present study, we develop a DNS database of C–P flows, which covers a wide range of flow conditions, at Reynolds numbers larger than considered by Kuroda *et al.* (1993). The objective of the paper is to shed light on the global turbulence organization in this class of flows, and quantitatively address the scaling of the energy-carrying motions. For this purpose, we will investigate the main mechanisms responsible for momentum exchange, embodied by streaks, to verify possible similarities with streaky motions in homogeneous shear flows. Furthermore, we will focus on the large-scale motions in the channel core and try to establish a quantitative relationship (in terms of imprinting and modulation) with the organization of the near-wall structures.

This paper is organized as follows. The numerical methodology and the test cases are presented in § 2. The organization of the various flows is studied in § 3 and § 4, where we analyse, respectively, the statistics of the velocity field and the geometry of the streaks. The interactions between the fine-grained near-wall turbulence and the large-scale structures in the channel core are addressed in § 5. Concluding remarks are given in § 6.

2. Numerical methodology

We solve the non-dimensional Navier–Stokes momentum equations for a divergence-free velocity field:

$$\left.\begin{aligned} \frac{\partial u_j}{\partial x_j} &= 0, \\ \frac{\partial u_i}{\partial t} + \frac{\partial u_i u_j}{\partial x_j} &= -\frac{1}{\rho}\frac{\partial p}{\partial x_i} + \nu \frac{\partial^2 u_i}{\partial x_j \partial x_j} - H\,\delta_{i1}, \end{aligned}\right\} \tag{2.1}$$

where H is the (negative) pressure gradient required to maintain a constant flow rate, u_i $(i = 1, 2, 3)$ is the component of the velocity vector in the ith direction, ρ is the density (assumed to be uniform), p is the pressure, and ν is the kinematic viscosity. The Navier–Stokes equations have been discretized in an orthogonal coordinate system (x_1, x_2, x_3, for the streamwise, wall-normal and spanwise directions, respectively) using staggered central second-order finite-difference approximations, whereby kinetic energy is globally conserved in the inviscid limit. The details of the numerical method are reported in Orlandi (2000).

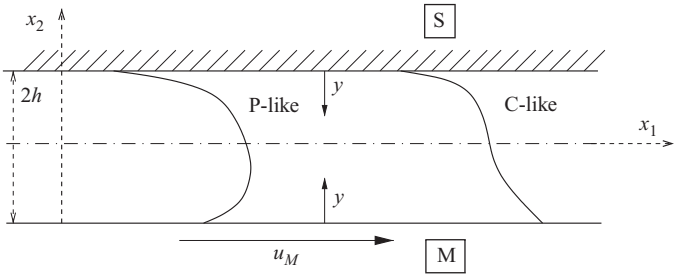

FIGURE 1. Sketch of mean velocity profiles in Poiseuille-like and Couette-like flows.

A sketch of the flow configuration, showing the reference system and typical mean velocity profiles, is depicted in figure 1. The boundary conditions at the lower (moving) wall, indicated by the subscript M, are applied by forcing a constant value (u_M) for the streamwise velocity. On the upper (stationary) wall, indicated by the subscript S, all three velocity components (hereafter also denoted as u, v, w) are set to zero.

The controlling parameter for the flow under consideration is the ratio of the shear stress at the two walls $\gamma = \tau_M/\tau_S$. With no loss of generality, one can always assume $-1 \leqslant \gamma \leqslant 1$. Couette-like flows are obtained for $\gamma > 0$, whereas Poiseuille-like flows are recovered for $\gamma < 0$. Specifically, pure Couette and Poiseuille flows correspond to $\gamma = 1$ and $\gamma = -1$, respectively. Flows with $\gamma \approx 0$ (hereafter referred to as shear-less) are of special interest, as they exhibit nearly zero mean shear at the moving wall, and can thus be used as a model for the understanding of turbulent flows near separation. Under such conditions, the wall affects the core flow only through the impermeability condition, and the coherent structures that are observed near the moving wall significantly differ from those found in canonical channel flow.

The simulations have been performed in a computational box with size $L_1 = 12\,\pi h$ in the streamwise and $L_3 = 4\,\pi h$ in the spanwise directions, h being the channel half-height. Such a large computational box is dictated by the need to accommodate very large coherent structures in the inner part of the channel, especially in the case of Couette-like flows (Bech *et al.* 1995). The computational domain has been discretized with $N_1 \times N_2 \times N_3 \equiv 1024 \times 256 \times 512$ cells in the x_1, x_2, x_3 directions, respectively. In the following, x_2 is used to denote the vertical coordinate ($-1 \leqslant x_2/h \leqslant 1$, $x_2/h = -1$ corresponding to the moving wall, and $x_2/h = 1$ to the stationary wall), whereas y is used to indicate the distance from the nearest wall ($y = \min(h - x_2, h + x_2)$, with $0 \leqslant y/h \leqslant 1$).

Simulations representative of the entire allowed range of γ have been performed. The flow case P is a canonical channel flow with two stationary walls ($\gamma = -1$); flow case P1 corresponds to a Poiseuille-like flow with reduced shear; flow case SL is representative of a shear-less flow ($\gamma \approx 0$); flow cases C1 and C are Couette-like flows, the latter being very close to pure Couette flow. The main flow parameters (u_M, γ and the friction Reynolds numbers at the moving and the stationary wall, Re_{τ_M}, Re_{τ_S}) are reported in table 1.

The simulations have been initiated with a laminar parabolic Poiseuille velocity profile, with maximum velocity u_p at the centreline, and bulk velocity $u_b = 2/3\,u_p$. The calculations have then been time-advanced by forcing constant mass flux through the channel in such a way that u_b does not vary with time. All the simulations reported in the present study have been performed at $Re = u_p h/\nu = 7200$, the corresponding bulk Reynolds number being $Re_b = u_b h/\nu = 4800$. After an initial transient (lasting

Flow case	u_M/u_p	γ	$Re_{\tau M}$	$Re_{\tau S}$	Line style
P	0	−1	284	284	——·——
P1	0.5	−0.24	128	261	– – – – –
SL	0.8	0.01	26	255	·–·–·–
C1	1.0	0.27	130	250	—— ——
C	1.3	0.98	242	245	· · · · · ·

TABLE 1. Flow parameters for DNS of C–P flows. $\gamma = \tau_M/\tau_S$, $Re_{\tau M,S} = u_{\tau M,S}h/\nu$, $u_{\tau M,S} = (|\tau_{M,S}|/\rho)^{1/2}$.

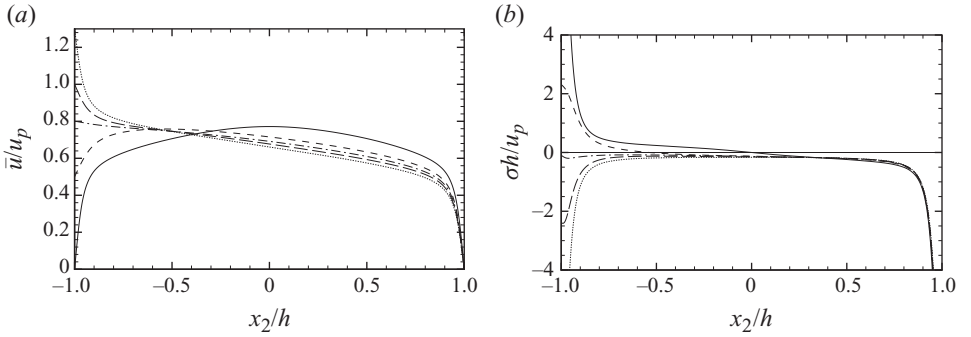

FIGURE 2. Distributions of (*a*) mean velocity ($\overline{u}$) and (*b*) mean shear rate ($\sigma = \mathrm{d}\overline{u}/\mathrm{d}x_2$). Lines: ——, P; – – –, P1; ·–·–, SL; ——, C1; · · · ·, C.

approximately 100 time units h/u_p) the pressure gradient starts to fluctuate about a nearly constant value ($\overline{H}$). After the end of this transient, 200 flow samples have been collected at unit time intervals, which is sufficient to guarantee statistical convergence of all properties reported in the paper.

3. Velocity statistics

Fully developed C–P flows are characterized by balance between the streamwise pressure gradient and the cross-stream shear-stress gradient, expressed by the mean axial momentum equation

$$\frac{\mathrm{d}\tau}{\mathrm{d}x_2} = \frac{\tau_S - \tau_M}{2h} = \frac{\tau_S(1-\gamma)}{2h} = \overline{H} \leqslant 0, \tag{3.1}$$

where the total shear stress (τ) is the sum of the viscous shear stress $\rho\nu\sigma$ ($\sigma = \mathrm{d}\overline{u}/\mathrm{d}x_2$ is the mean shear), and the Reynolds shear stress $-\rho\,\overline{u'v'}$ (Reynolds-averaged quantities are hereafter indicated by an overbar and fluctuations by the prime symbol). Note that the two forcing mechanisms are different in principle because the pressure drop between the entrance and the exit of the duct is globally felt by the flow, whereas the movement of one wall locally forces momentum, that is transmitted into the core flow through viscous forces and turbulent transport.

The distributions of the mean velocity and the mean shear stress are reported in figure 2. When the lower wall is put into motion, the wall stress τ_M gradually decreases and the location where maximum velocity is attained shifts from the channel centreline

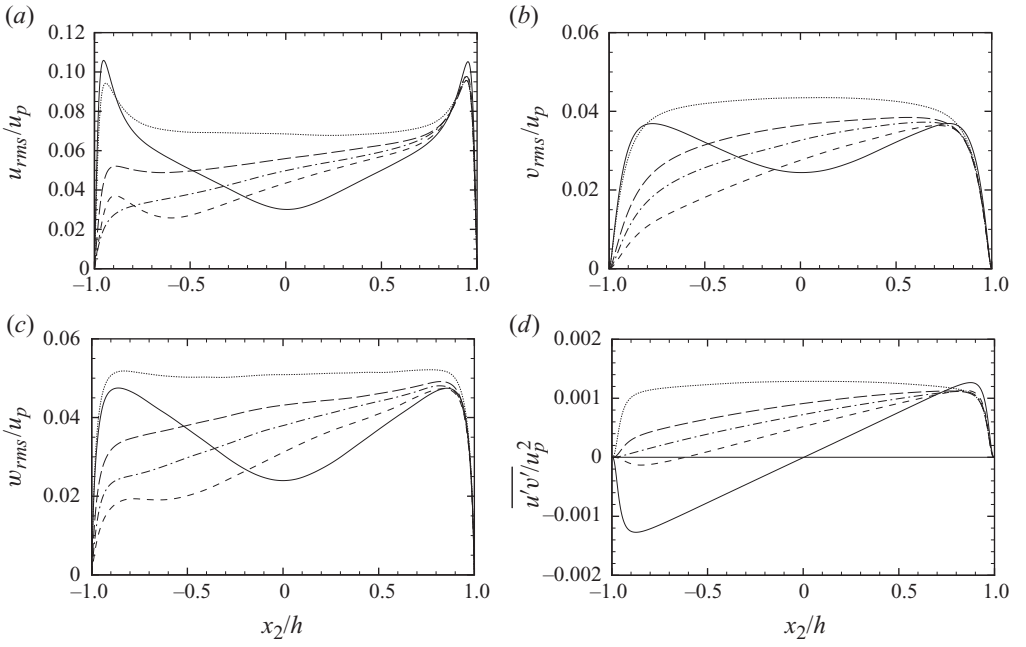

FIGURE 3. (*a–d*) Statistics of velocity fluctuations across the channel. Lines: ——, P; – – –, P1; ·–·–, SL; ——, C1; · · · ·, C.

towards the moving wall. When $u_M/u_p \approx 0.8$, the maximum velocity is first attained at the moving wall. This situation corresponds to a locally shear-less motion, for which the only effect of the wall is the suppression of the wall-normal motions (blocking effect). Further increase of u_M leads to Couette-like flows, for which no change of sign of the mean shear occurs.

The root-mean-square (r.m.s.) velocity fluctuations and the Reynolds shear stress are reported in figure 3 in computational units. Minor sensitivity to the wall motion is observed in close proximity of the stationary wall, where the flow is dominated by the local shear, and reasonable collapse of the flow statistics is observed. Significant differences are found near the channel centreline, where a monotonic increase of all the Reynolds stress components with γ is found. The velocity fluctuations in the lower half of the channel are apparently strongly affected by the friction at the moving wall, and a definite trend with γ is not observed. Also note that the near-wall peak of the streamwise velocity fluctuations, associated with the turbulence regeneration cycle, vanishes in the case of the SL flow.

The possible establishment of a universal distribution of velocity fluctuations has been explored by scaling the flow properties with respect to viscous units taken at the nearest wall, i.e.

$$u_{\tau M,S} = \nu^{1/2}\,|\sigma|_{M,S}^{1/2}, \quad \ell_{M,S} = \nu/u_{\tau M,S}, \tag{3.2}$$

where $u_{\tau M,S}$ and $\ell_{M,S}$ are, respectively, the friction velocity and the viscous length scale based on the local shear at the moving (M) and stationary (S) walls. Note that, in the singular case of vanishing wall shear stress, reference velocity and length scales can be conveniently defined on the basis of the imposed pressure gradient

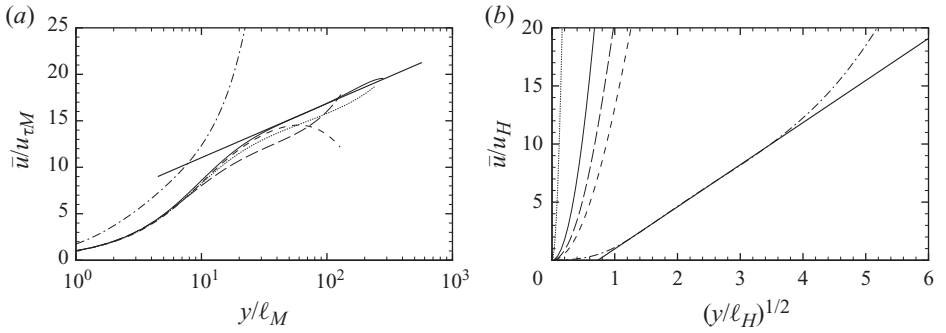

FIGURE 4. Mean velocity profiles near the moving wall scaled in (*a*) wall units and (*b*) pressure units. The distance from the wall ($y = h + x_2$) is denoted by y. The thick solid line indicates the standard log-law for Poiseuille flow ($u^+ = 1/k \log y^+ + B$, with $k = 0.41$, $B = 5.2$) in (*a*), and the square root law ($u/u_H = 2/k^*(y/\ell_H)^{1/2} + B^*$, with $k^* = 0.55$, $B^* = -2.65$) in (*b*). Lines: ——, P; – – –, P1; · – · –, SL; — —, C1; · · · ·, C.

(Schlichting & Gersten 2000)

$$u_H = \left(-\frac{\nu}{\rho}\overline{H}\right)^{1/3}, \quad \ell_H = \nu/u_H. \tag{3.3}$$

The mean velocity distributions near the moving wall are reported in figure 4 in friction and pressure scaling. The scaling based on the wall friction gives rise, limited to the case of the C and P flows, to a narrow layer (if any) with near-logarithmic scaling ($u^+ = 1/k \log y^+ + B$). As pointed out by many previous authors, the log-law constant (provided an overlap layer exists at this low Reynolds number) is different between C and P flows, owing to the different pressure gradient. Specifically, we find $B = 4.7$ for the C flow, which is in perfect agreement with the DNS study of Bech *et al.* (1995), and the standard value $B = 5.2$ for the P flow. A sizeable region with square-root variation of the mean velocity is recovered in the case of the SL flow (figure 4*b*), when pressure scaling is used.

Figures 5 and 6 give the Reynolds stress components scaled in wall units near the two walls. For a consistency check, in the figures we also report the fully developed channel flow data by Hoyas & Jiménez (2006), at two Reynolds numbers, one higher and one lower than the present study. As expected, the reference DNS data envelope our P flow data. With regard to the flow statistics near the stationary wall (figure 5), a rather weak sensitivity to the movement of the opposing wall is found for the streamwise velocity fluctuations, whereas larger differences are found for the cross-stream ones. In all cases, a systematic trend for velocity fluctuations to increase with γ is observed, which resembles the effect of increasing the Reynolds number in the P flow case (recalling table 1, $Re_{\tau S}$ here is nearly the same for all cases). This behaviour suggests the existence of a different coupling between the near-wall region and the inner channel dynamics for P-like and C-like flows, which will be investigated later. Larger spread of the curves and stronger deviations from the canonical channel behaviour are observed near the moving wall (figure 6), where the statistics for the P and the C flow cases are identical to those for the stationary wall. In this case, no definite trend with γ is observed.

Flatter distributions of the velocity fluctuations are found introducing a viscous scaling based on the local value of the mean shear

$$u_{\tau L}(x_2) = \nu^{1/2}\,|\sigma(x_2)|^{1/2}, \quad \ell_L(x_2) = \nu/u_{\tau L}(x_2). \tag{3.4}$$

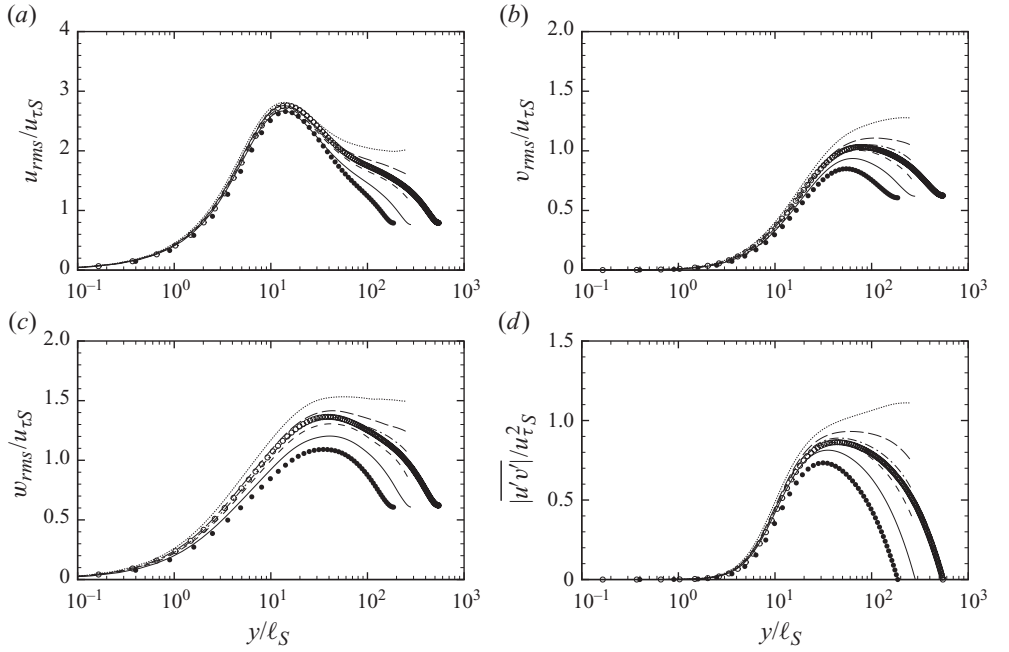

FIGURE 5. (*a–d*) Statistics of velocity fluctuations near the stationary wall in wall units (only data for $0 \leqslant x_2/h \leqslant 1$ are shown, $y = h - x_2$). Symbols (Hoyas & Jiménez 2006) correspond to Poiseuille flow at (●) $Re_\tau = 180$ and (○), $Re_\tau = 550$. Lines: ——, P; – – –, P1; – · – · –, SL; — —, C1; · · · ·, C.

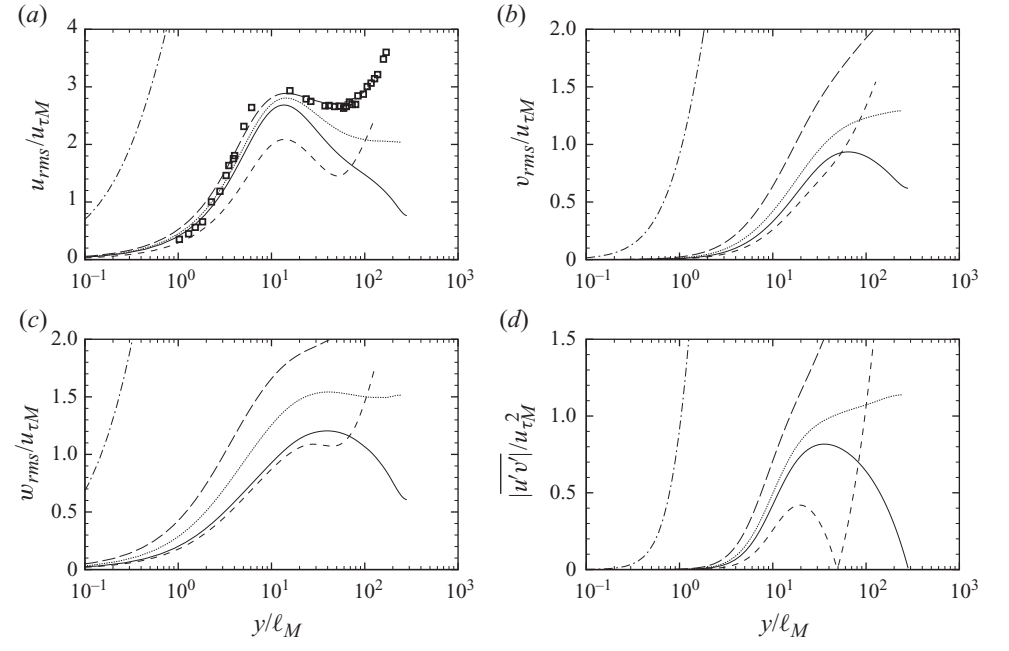

FIGURE 6. (*a–d*) Statistics of velocity fluctuations near the moving wall in wall units (only data for $-1 \leqslant x_2/h \leqslant 0$ are shown, $y = h + x_2$). Square symbols indicate experimental data by Nakabayashi *et al.* (2004) at $\gamma = 0.29$, $Re_{\tau M} = 103$. Lines: ——, P; – – –, P1; – · – · –, SL; — —, C1; · · · ·, C.

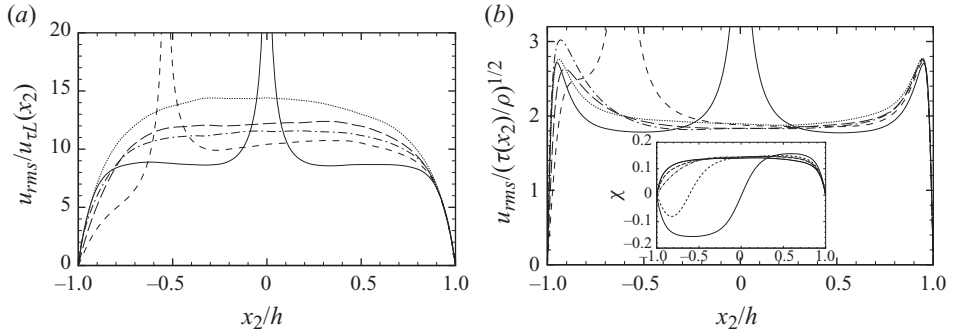

FIGURE 7. Streamwise r.m.s. velocity fluctuations scaled by (*a*) local viscous friction and (*b*) local total friction. The inset in (*b*) gives the distribution of the structure parameter $\chi = \overline{u'v'}/\overline{u_i'u_i'}$. Lines: ——, P; – – –, P1; · – · –, SL; — —, C1; · · · ·, C.

Obviously, the classical wall scaling is recovered near the two walls. The scaling (3.4) amounts to assuming that the flow is locally similar to a uniformly sheared turbulent flow subjected to the local mean velocity gradient. In the case of uniformly sheared homogeneous turbulence it was found that $u_{rms}/u_{\tau L} \approx 3$–7 (Lee *et al.* 1990). The distribution of the scaled r.m.s. streamwise velocity fluctuations is reported in figure 7(*a*), where the wall-normal coordinate is not scaled. Interestingly, away from the walls and from zeros of the mean shear, the scaled velocity distributions remain approximately constant across a large part of the channel, for all the flow cases. However, the plateau value is different for the different flow cases, and it steadily increases with increasing γ. This stands to indicate that, while turbulence inside the channel can be approximately regarded as uniformly sheared turbulence subjected to the local mean shear, deviations from universality still occur, which may be related either to the effect of the imposed pressure gradient, being different from case to case, or to differences in the global flow dynamics, to be discussed in § 5. Similar distributions are also found for the other fluctuating velocity components, not shown here. As seen in figure 7(*b*), even better collapse is achieved (as also observed by El Telbany & Reynolds 1980) using the friction velocity based on the total stress $(\tau/\rho)^{1/2}$ to scale the velocity fluctuations. In this case, nearly universal values are found for the r.m.s. velocity components in the core of the channel. Observing that, away from walls $\tau \approx -\rho\overline{u'v'}$, constancy of the velocity statistics in the total stress scaling implies constancy of the structure parameter (Klebanoff 1955), $\chi = \overline{u'v'}/\overline{u_i'u_i'}$, which is found to be $|\chi| \approx 0.13$–0.15 (see inset to figure 7*b*).

The budgets of the turbulence kinetic energy ($k = \overline{u_i'u_i'}/2$) near the two walls are considered next:

$$\underbrace{-\sigma\,\overline{u'v'}}_{\mathscr{P}} \underbrace{-\frac{1}{\rho}\frac{\mathrm{d}\,\overline{v'p'}}{\mathrm{d}x_2}}_{\Pi} \underbrace{-\frac{\mathrm{d}\,\overline{v'k}}{\mathrm{d}x_2}}_{T} \underbrace{+\nu\frac{\mathrm{d}^2k}{\mathrm{d}x_2^2}}_{V} \underbrace{-\nu\overline{\frac{\partial u_i'}{\partial x_j}\frac{\partial u_i'}{\partial x_j}}}_{\varepsilon} = 0, \tag{3.5}$$

where $\mathscr{P}$, Π, T , V and ε are the terms associated, respectively, with production, pressure transport, turbulent transport, viscous diffusion and dissipation. Very similar distributions for all cases (not shown) are found near the stationary wall, with near-wall balance between viscous diffusion and dissipation, and balance between production and dissipation far from it, as for canonical Poiseuille flow. Near the moving wall (figure 8), near-canonical behaviour is again found for both the P and

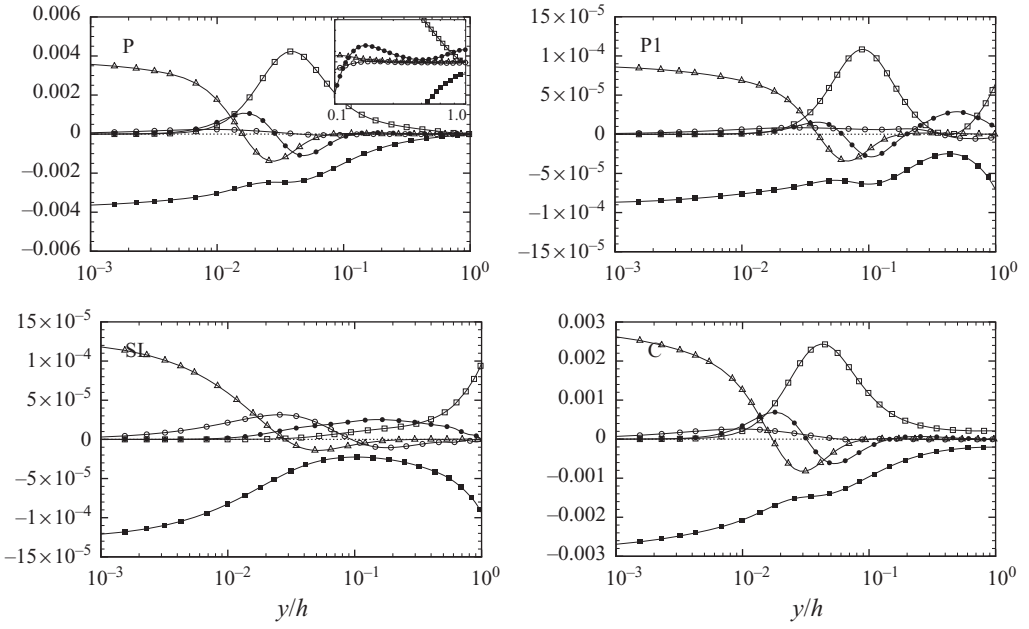

FIGURE 8. (*a–d*) Turbulence kinetic energy budget near the moving wall (all terms scaled with respect to u_p^3/h, $y = h + x_2$). □, $\mathscr{P}$; ○, Π; ●, T; △, V; ■, ε. The inset in (*a*) shows a zoom near the channel centreline.

the C flow, with peak production occurring at $y/h = 0.04$–0.05 (corresponding to $y^+ = 10$–12). The main effect of reducing the mean shear at the moving wall is the suppression of the production term in its vicinity, and the near-wall production peak indeed vanishes in the case of the SL flow. In that case, the importance of the turbulent transport term (which is everywhere positive) suggests that near-wall turbulence is dominated by the transport of kinetic energy from the channel core. Balance between turbulent transport and dissipation is observed at the channel centre for the P flow (see inset of figure 8*a*), where, owing to the annihilation of the mean shear, sustaining turbulence requires inward turbulence kinetic energy flux from the two walls. For all the other cases, equilibrium between production and dissipation is recovered near the channel centre, since the mean shear is not zero (recalling figure 2*b*).

4. Streaks geometry

The velocity statistics illustrated in the previous section are here complemented with the analysis of the geometrical organization of the velocity field. The occurrence of momentum streaks can be conveniently appreciated from the inspection of the velocity fluctuation field in wall-parallel planes, reported in figures 9–11. A streaky pattern is always observed near the stationary wall, as well as near the moving wall, except for the SL flow. Streaks (with apparently much larger size) are also observed at the channel centreline, except for the P flow. These observations can be explained recalling that for non-uniformly sheared flows (Lam & Banerjee 1992), streaks can only be sustained if the ratio of the local turbulence kinetic energy production to the local viscous dissipation is at least of order unity. Applying this criterion to the C–P class of flows leads to the map depicted in figure 12 which, consistent with the

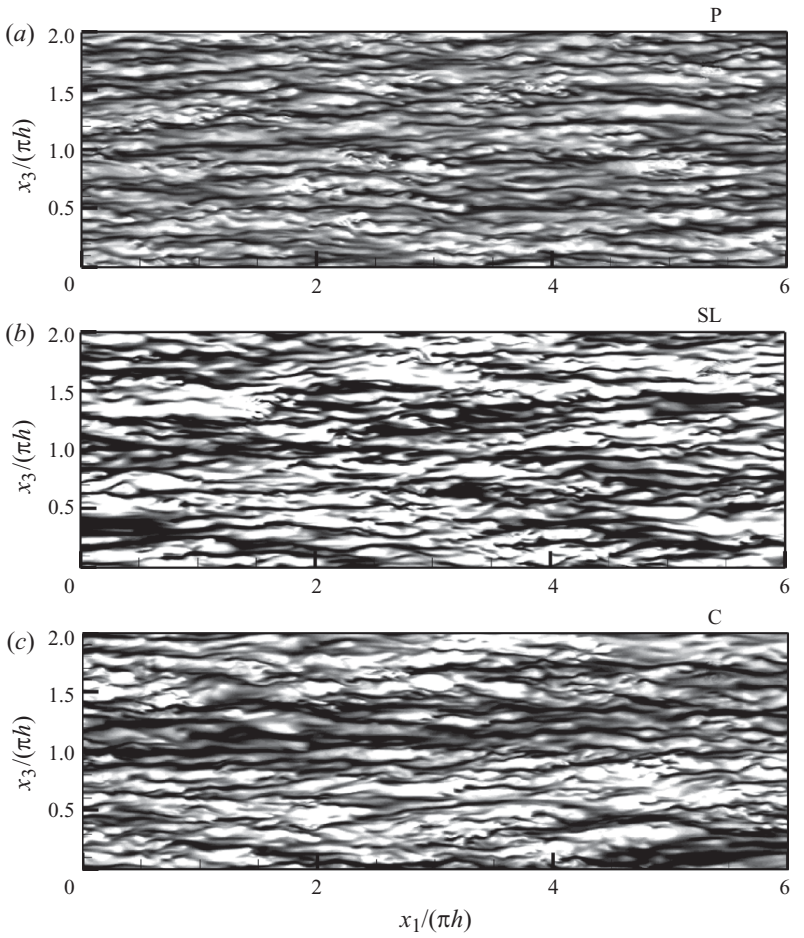

FIGURE 9. (*a–c*) Contours of streamwise velocity fluctuations in a parallel plane near the stationary wall (taken at a distance $y/h = 0.04$, where $\mathscr{P}/\varepsilon = 1.72, 1.73$ and 1.69, respectively). Sixteen contour levels are shown, $-1.5 < u'/u_{rms} < 1.5$ (grey scale from black to white). Only a quarter of the full domain is shown.

instantaneous visualizations, suggests that streaks are not expected to occur in the lower part of the channel for the SL flow, and near zeros of the local mean shear for the P and P1 flows.

Turning to the flow visualizations more carefully, several additional observations can be made. Looking at the moving wall (figure 11), it is clear that the larger the spanwise size of the streaks the smaller is the wall shear. Furthermore, comparing the P and C flows (which have approximately the same absolute value of the wall shear), one can see a similar size of the streaks. However, closer inspection highlights a roughly uniform distribution of streaks in the spanwise direction for the P flow, whereas the C flow apparently exhibits (both near the stationary and the moving wall) streaky organization on two typical length scales, one similar to that of the P flow streaks, and one typical of the C flow in the channel core (compare with figure 10*c*). As will be demonstrated in the next section, this phenomenon is caused by an imprinting imparted by large-scale events in the channel core onto the near-wall motions. It is also interesting to note the differences between the SL flow near the

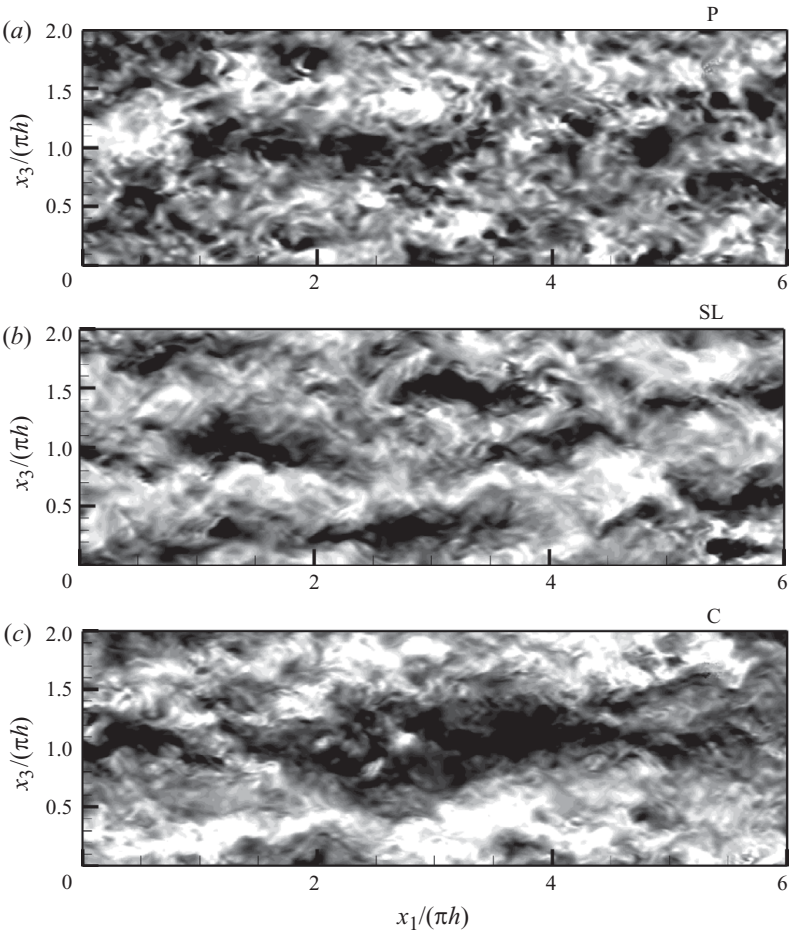

FIGURE 10. (*a–c*) Contours of streamwise velocity fluctuations at the channel centreplane ($x_2 = 0$), where $\mathscr{P}/\varepsilon = 0$, 1.04 and 1.01, respectively. Sixteen contour levels are shown, $-1.5 < u'/u_{rms} < 1.5$ (grey scale from black to white). Only a quarter of the full domain is shown.

moving wall and the P flow at the channel centreline, which both have $\mathscr{P}/\varepsilon \approx 0$. Although streaks are absent in both cases, the pattern of the velocity fluctuations is quite different, owing to the blocking effect of the moving wall in the SL flow.

The spanwise streak spacing (say λ_z) is usually inferred (Kim, Moin & Moser 1987) from inspection of the two-point autocorrelation of the streamwise velocity fluctuations. It is known that in the near-wall region of wall-bounded flows a distinct negative correlation peak occurs for spanwise separations $\Delta z^+ \approx 50$, which implies $\lambda_z^+ \approx 100$ (Kim *et al.* 1987). On the other hand, in the case of uniformly sheared flows, Lee *et al.* (1990) showed that $\lambda_z \approx 120$–$200\,\ell_L$. The autocorrelation coefficient of streamwise velocity fluctuations is reported in figure 13 for points located near the moving wall (figure 13*a*) and at the channel centreline (figure 13*b*). As expected from visual analysis of the velocity fields, the two-point correlations exhibit a prominent negative peak for most cases, indicating the occurrence of an alternating pattern of low- and high-speed streaks, which grow in size moving away from the wall. A distinct minimum is not found near the moving wall for the SL flow and near the centreline

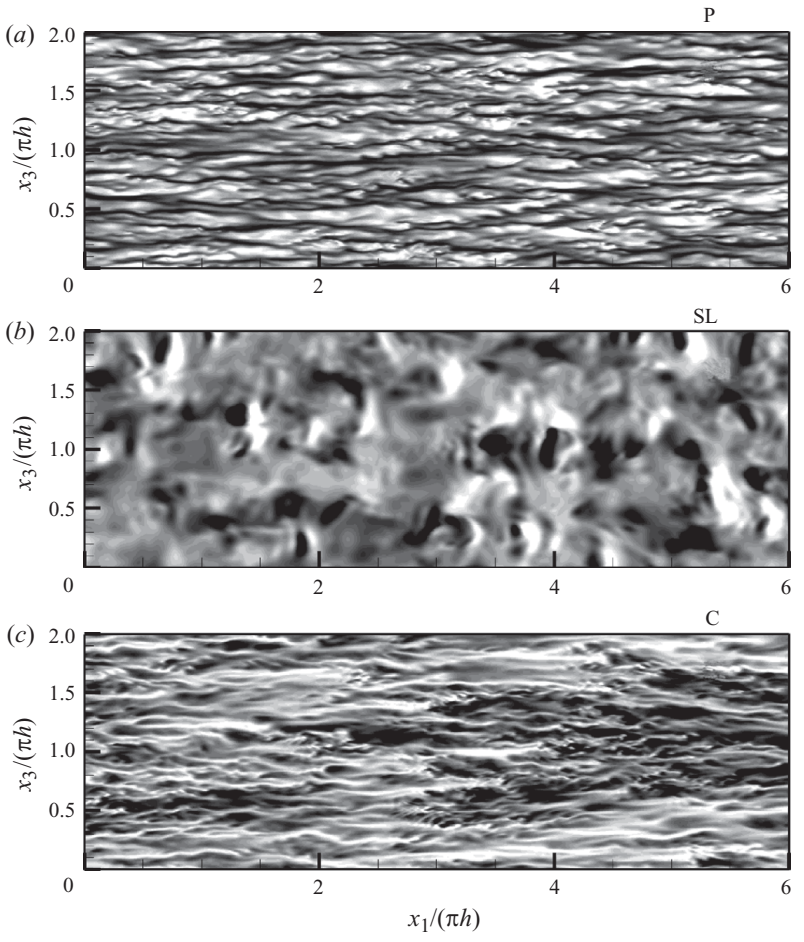

FIGURE 11. (*a–c*) Contours of streamwise velocity fluctuations in a parallel plane near the moving wall (taken at a distance $y/h = 0.04$, where $\mathscr{P}/\varepsilon = 1.72, 0.093$ and 1.69, respectively). Sixteen contour levels are shown, $-1.5 < u'/u_{rms} < 1.5$ (grey scale from black to white). Only a quarter of the full domain is shown.

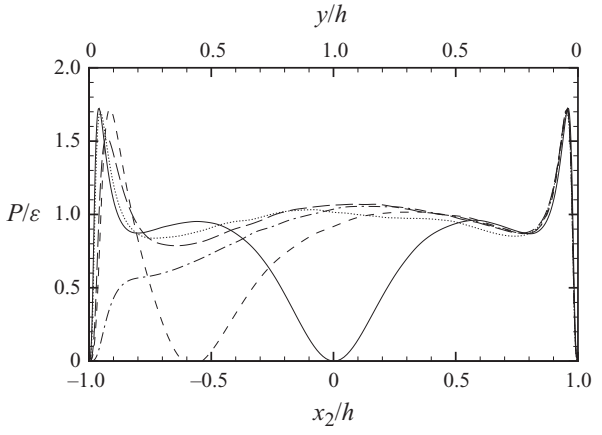

FIGURE 12. Distribution of local production-to-dissipation ratio. Lines: ——, P; – – –, P1; ·–·–, SL; ——, C1; · · · ·, C.

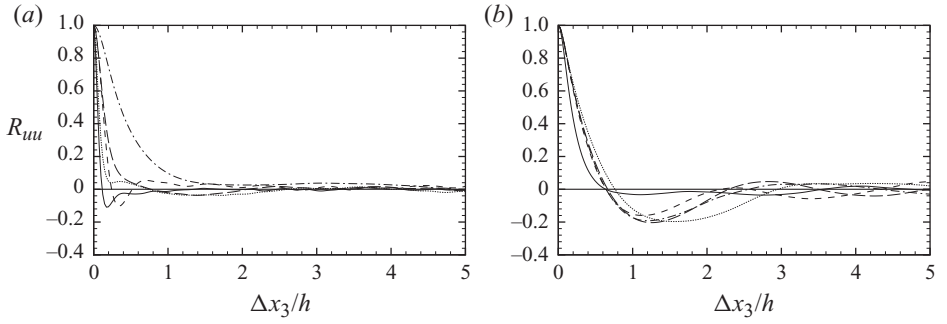

FIGURE 13. Auto-correlation coefficient of streamwise velocity fluctuations in the spanwise direction taken (*a*) near the moving wall and (*b*) at the channel centreline. Lines: ——, P; – – –, P1; · – · –, SL; ——, C1; · · · ·, C.

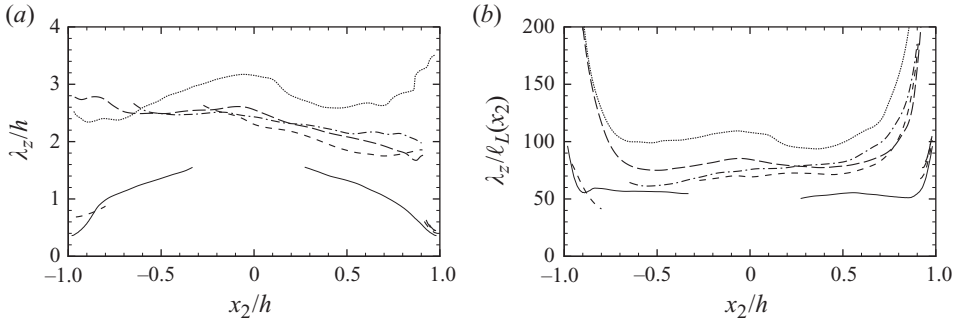

FIGURE 14. Mean spanwise streak spacing, estimated from absolute minimum of the spanwise auto-correlation of u. The spacing is scaled with respect to outer units in (*a*) and with respect to local viscous units in (*b*). Lines: ——, P; – – –, P1; · – · –, SL; ——, C1; · · · ·, C.

for the P flow, confirming the absence of a streaky pattern. Close examination of figure 13(*a*) in the case of C flow shows the presence of a plateau (rather than a clear minimum) in the two-point correlation at $\Delta x_3 \approx 0.33h$ (amounting to $\Delta x_3 \approx 81\,\ell_M$), and a primary negative peak at $\Delta x_3 \approx 1.6h$, which is approximately the same location as in figure 13(*b*). This is suggestive of the presence of two characteristic scales for the streaks and supports the observations made in figure 11. In this case, the correlation minimum associated with the inner-layer dynamics is masked by the minimum associated with large-scale organization in the outer layer.

To get an insight into the change of scales of the momentum-carrying motions across the channel, we have determined the absolute negative minimum of the spanwise two-point correlations (wherever it occurs) at all wall-normal stations. Comparison of the calculated streak spacing for the P flow with available channel data (Smith & Metzler 1983; Kim *et al.* 1987) shows excellent agreement in the inner layer, with spacing of about 100 wall units at the wall, which increases with the wall distance. The distributions of λ_z for all the flow cases is reported in figure 14. Note that the curves are interrupted where the minimum search algorithm fails, which is indicative of the local inhibition of streaks. Also note that outer scaling is used in figure 14(*a*), whereas the local scaling (3.4) is used to report the same data in figure 14(*b*). Figure 14(*b*) supports the capability of local viscous scaling to yield

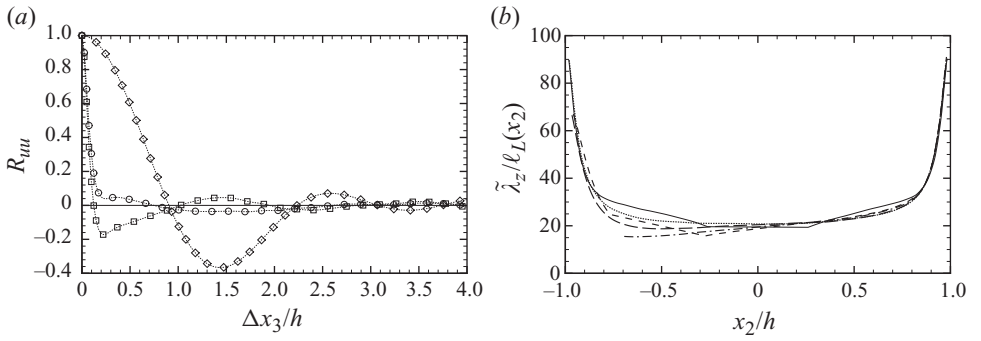

FIGURE 15. Analysis of filtered streamwise velocity fields. (*a*) C flow: autocorrelation coefficient near the moving wall determined from full velocity field (○), low-pass-filtered velocity field (◇), and high-pass-filtered velocity field (□). The low- and high-pass-filtered velocity fields contain 33 % and 67 % of the total energy, respectively. (*b*) Mean streak spacing in local viscous units determined from the high-pass-filtered fields. Lines: ——, P; – – –, P1; · – · –, SL; — —, C1; · · · ·, C.

relatively flat distributions of flow statistics across large part of the channel, even though, as also observed for the velocity fluctuation statistics, the constant may change from flow to flow, with variations in the range $50 \leqslant \lambda_z/\ell_L \leqslant 100$. The closest value to those reported by Kim *et al.* (1987) for homogeneous turbulence is found in the C flow (in which case $\lambda_z/\ell_L \approx 100$), consistent with the fact that Couette flow can be assimilated to a homogeneously sheared flow in the core of the channel. In this case (the results are not shown), using a local scaling based on the total stress yields more scattered results than using the mean shear.

It is worth noting that, when reported in local viscous units, the streak spacing has a strong peak in the vicinity of the walls in the case of C-like flows, which requires some explanation. In this respect, we recall that the spacings have been determined solely on the basis of the absolute negative minimum of R_{uu}. However, as previously mentioned, a secondary minimum in the autocorrelations is likely to be present for C-like flows, which is not accounted for in figure 14. To bring out such secondary minima we have high-pass filtered the velocity fields in the spanwise direction, using a sharp Fourier cut-off at the wavelength h, which (given the spanwise length of the domain $L_3 = 4\pi h$) approximately amounts to retaining only the Fourier modes of the velocity field from 12 to $N_3/2$. The autocorrelation coefficient near the moving wall (only shown for the C flow) and the mean streak spacing determined from the filtered velocity fields are plotted in figure 15. The figure must be interpreted with caution, since the filtering operator does not strictly preserve the structure of the flow field. However, the negative correlation peak observed for the high-pass-filtered C flow in figure 15(*a*), now much more evident, matches well the position of the plateau seen in figure 13, and the negative peak correlation found in the low-pass-filtered fields occurs at the same location as the global minimum in the unfiltered fields. This is a compelling confirmation that near-wall streaks for the C flow are characterized by two distinct length scales. The distribution of the mean streaks spacing determined from the autocorrelations of the high-pass-filtered velocity fields, reported in figure 15(*b*), further suggests that the spanwise spacing of small streaks near the walls obeys a nearly universal scaling. The collapse observed in figure 15(*b*) in the core of the channel (where large-scale structures dominate) does not have physical significance, since all energy-containing scales of motion have been filtered out.

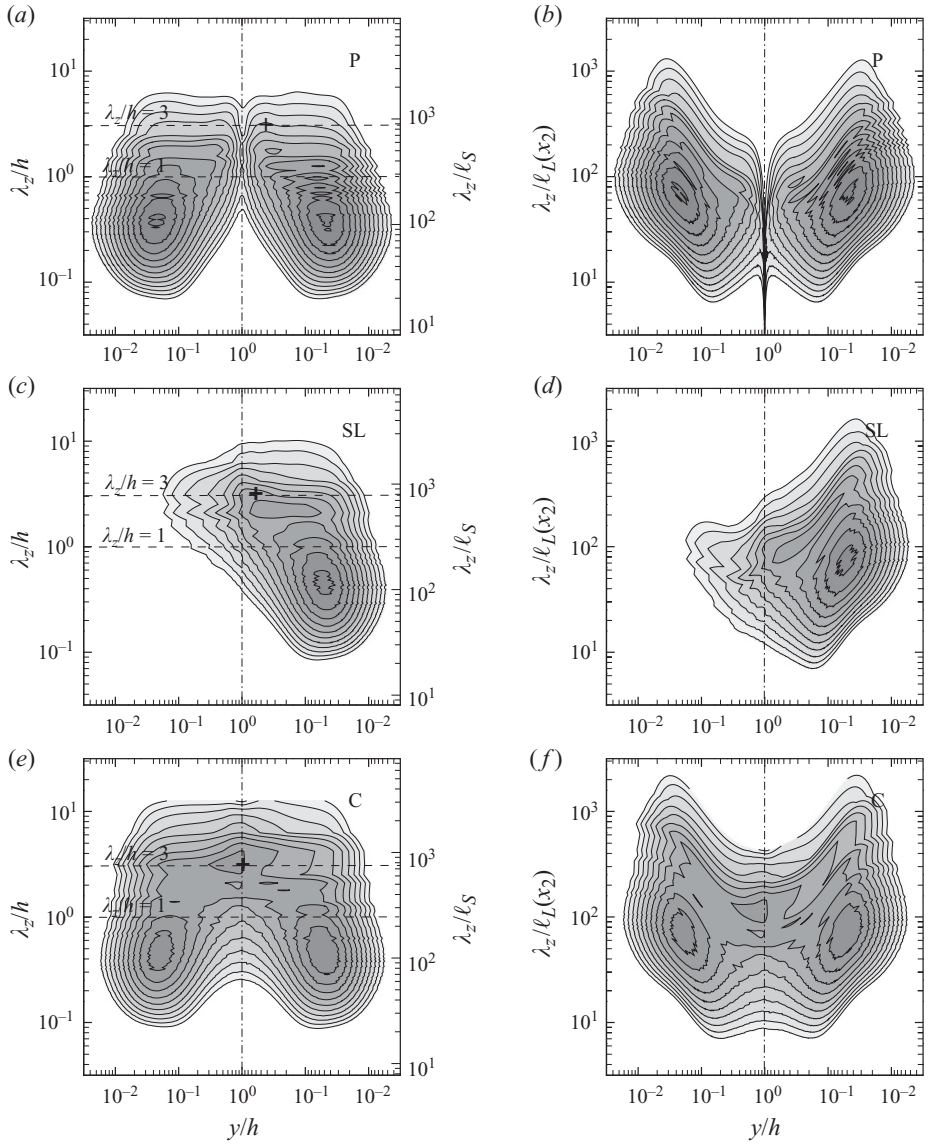

FIGURE 16. Pre-multiplied spectra of streamwise velocity fluctuations in the spanwise direction ($k_z E_{uu}$) at various wall-normal locations. The distance from the nearest wall (y) is reported on the horizontal axis in logarithmic scale to emphasize the near-wall behaviour. The spanwise wavelength λ_z is scaled with respect to either (a, c, e) the channel height or (b, d, f) the local viscous length scale. The channel centreline is shown by a vertical dot-dashed line. Sixteen logarithmically spaced contour levels from $10^{-4}u_p^2$ to $10^{-2}u_p^2$ are shown. The black crosses denote the peak locations of the spectral densities for $\lambda_z/h = 3$.

5. Inner/outer layer interactions

5.1. *Energy spectra*

The information contained in the autocorrelations of u' can also be usefully represented in Fourier space in terms of the pre-multiplied energy spectra, and reported as a function of the spanwise wavelength at all the vertical stations, as done in figure 16. As pointed out by Hutchins & Marusic (2007), this type of representation

yields immediate understanding of the energetic relevance of the various scales of motions at different distances from the wall, and it was therefore used to assess the signature of super-structures in turbulent boundary layers (Hutchins & Marusic 2007) and the occurrence of VLSM in channels and pipes (Kim & Adrian 1999; Monty *et al.* 2009) at high Reynolds number. In experiments, spectra are usually taken in the streamwise direction by applying Taylor's hypothesis to time series at a given off-wall station. Here spectra are directly taken in physical space, which removes any uncertainty associated with the application of Taylor's hypothesis to the large scales of motion (del Álamo & Jiménez 2009).

In the case of the P flow, figure 16 shows the presence of two distinct peaks in the spanwise power spectral density, specular with respect to the centreline, whose energy is concentrated about $\lambda_z \approx 0.39h$ (corresponding to $\lambda_z^+ \approx 110$). These peaks, which are located at a distance from the wall $y/h \approx 0.05$ (corresponding to $y^+ \approx 12$), are the typical signature of the inner-layer streaks regeneration cycle. Consistent with the moderate Reynolds number of the simulation, no obvious secondary peak is observed further away from the walls, associated with possible LSM, even though the characteristic scale of the energy-containing motions is seen to increase steadily with the wall distance. When the lower wall is set into motion, the primary effect is a depletion of energy in its proximity, associated with suppression of the streaks, until (SL flow) a low-wavenumber energy maximum forms in the upper part of the channel, which also extends its influence to the lower part. This modification suggests the occurrence of transfer of energy from the stationary to the moving wall, which is consistent with the previously observed increased importance of the turbulence transport term in that region. Finally, a global circulation establishes across the whole channel for the C flow, associated with the secondary energy peak (now at the channel centreline) having $\lambda_z \approx 3h$ ($\lambda_z^+ \approx 730$), and with the re-formation of the near-wall energy site at the moving wall. Note that a ridge in the spectrum departs from this secondary peak, which extends to the vicinity of both walls and supports significant influence of the outer motions on the near-wall ones, through a superposition (imprinting) mechanism. To further test the relevance of the local viscous scaling defined in (3.4), in figure 16(*b*, *d*, *f*) the spectral densities of u' are reported as a function of the locally scaled wavelength ($\lambda_z/\ell_L(x_2)$). Scaling the wavenumber has the evident effect of yielding a flatter distribution of the spectral peaks (at a given wall-normal station) across the channel, the peaks being clustered around $\lambda_z = 75$–$100\,\ell_L$, at least far from the walls. This observation further substantiates the previously noted relevance of the local mean shear in setting the length scales of the turbulence structures. A similar organization of the power spectral density is also observed in the streamwise spectra of u' (reported in figure 17), which reveal that the near-wall streaks (whenever they are present) have a length of about $3h$, corresponding to $\lambda_x^+ \approx 850$. The large-scale streaks observed in the core of the channel in C-like flows retain but a faint signature in the streamwise spectra, and their length, estimated on the basis of the weak spectral peak at the symmetry plane, is $\lambda_x \approx 10h$. In terms of local viscous units (figure 17*b*, *d*, *f*), the typical streamwise length of the streaks is found to be very nearly constant across the inner part of the channel for all flow cases, $\lambda_z \approx 450\,\ell_L$. Note that, because of the meandering nature of the streaks (Hutchins & Marusic 2007), this is likely to be a lower limit for the actual streaks length.

Based on the spanwise spectra, one can (more or less arbitrarily, given the lack of clear scale separation at the Reynolds number here dealt with) define a cutoff length scale to distinguish between small and large scales of motion. Looking at figure 16, it seems that $\lambda_z = h$ is a reasonable choice (at least in the case of the C

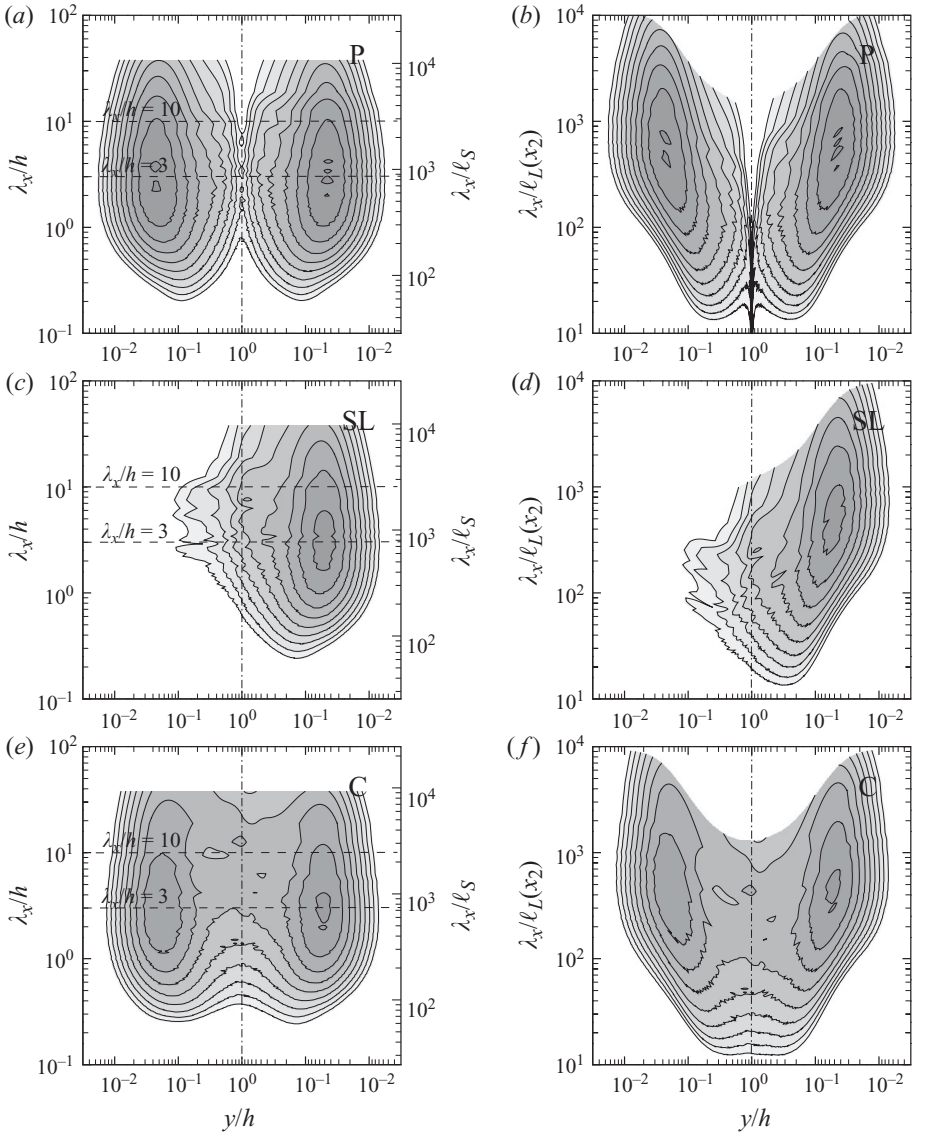

FIGURE 17. Pre-multiplied spectra of streamwise velocity fluctuations in the streamwise direction ($k_x E_{uu}$) at various wall-normal locations. Note that the distance from the nearest wall (y) is reported on the horizontal axis in logarithmic scale to emphasize the near-wall behaviour. The streamwise wavelength λ_x is scaled with respect to (a) the channel height and (b) the local viscous length scale. The channel centreline is indicated by a vertical dot-dashed line. Sixteen logarithmically spaced contour levels from $10^{-4}u_p^2$ to $10^{-2}u_p^2$ are shown.

flow) to discriminate between the inner-layer dynamics and the large-scale channel core circulation. The analysis of the low- and high-pass-filtered velocity fields can be used to explain the trends observed in the r.m.s. velocity fluctuations near the stationary wall in figure 5. In figure 18 we report (limited to the C and P flows) the variance of the filtered velocity components, to highlight the small-scale (high-pass) and the large-scale (low-pass) contributions. Note that the variance is here reported instead of the r.m.s. value, so that the two contributions add up to the variance of

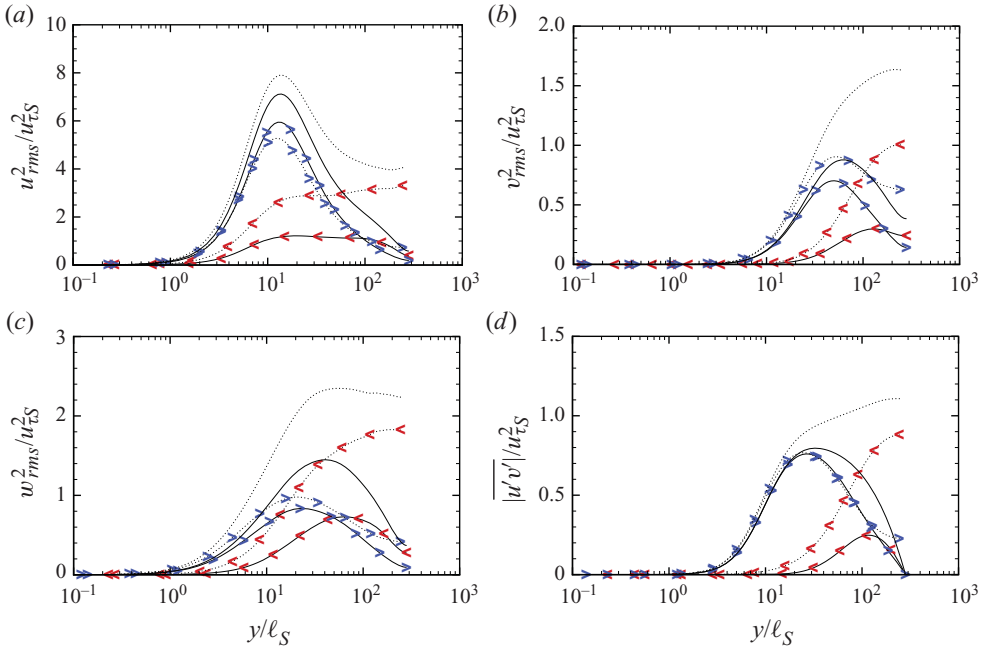

FIGURE 18. (Colour online available at journals.cambridge.org/flm) (*a–d*) Statistics of filtered velocity fluctuations near the stationary wall in wall units (only data for $0 \leqslant x_2/h \leqslant 1$ are shown, $y = h - x_2$). Symbols indicate statistics obtained from low-pass- (<) and high-pass- (>) filtered fields. Lines without symbols denote unfiltered data (as reported in figure 5). Lines: ——, P; · · · ·, C.

the unfiltered velocity signal. In the figure, we also report contributions of the low- and high-pass velocity fields to the Reynolds shear stress. A similar analysis was presented for boundary-layer flows by Marusic, Mathis & Hutchins (2010), but based on filtering in the time domain and limited to the streamwise velocity variance. The figure highlights several facts. First, it is found that the small-scale contribution to the r.m.s. of the three velocity components is similar for the two flows. This is a clear indication that the inner-layer dynamics is robust, and, in a first approximation, it is insensitive to the global flow geometry. As is well known, the nature of the near-wall velocity fluctuations associated with the small-scale dynamics is very anisotropic, with a prevalence of the streamwise velocity component. The contribution of the large-scale velocity field is found to be very small up to the buffer layer, but it always becomes dominant towards the channel core. Furthermore, the large-scale velocity fluctuations are found to be much more 'isotropic' (in the sense that the variance of the velocity components are of similar magnitude) than the small-scale ones, because they feel the blocking influence of wall-normal motions to a lesser extent (Townsend 1976). As a consequence, stronger influence of the large-scale motions is observed on the cross-stream velocity components, which explains the trends observed in figure 5. These conclusions also apply to the Reynolds shear stress, also reported in figure 18. Remarkable invariance of the small-scale contribution is found between the C and P flows, to an even greater extent than for the velocity variances. On the other hand, a substantial contribution from the large scales is found outside the buffer layer for the C flow.

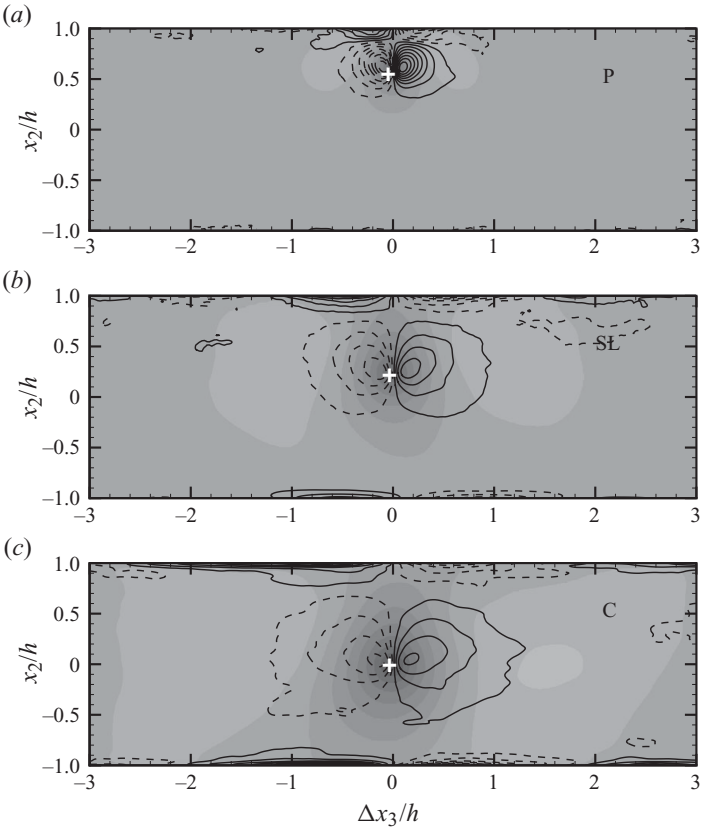

FIGURE 19. (*a–c*) Conditional expected fields associated with low-speed streaks ($u'/u_{rms} < -1.5$) at the outer low-wavenumber energy site (marked by a cross; see figure 16 for reference). Flooded contours correspond to streamwise velocity fluctuations (16 contour levels are shown, $-0.13 \leqslant u'/u_p \leqslant 0.13$, grey scale from black to white. Contour lines correspond to iso-levels of streamwise vorticity (16 contour levels are shown, $-0.3 \leqslant \omega_x h/u_p \leqslant 0.3$, dashed lines denoting negative values).

5.2. *Conditional eddies*

The physical mechanisms through which the large structures that arise within the channel modify the mechanisms of turbulence production near the walls can be understood by analysing the conditional average fields based on the presence of large-scale low-speed streaks, which are shown in figure 19. For this purpose, we consider reference points which are possibly representative of the large scales of motion, whenever they are present. Indeed, as previously noted, no genuine large-scale dynamics can be isolated for P-like flows, whereas an outer energy site emerges for the C-like flows, with the eventual formation of a distinct energy peak at the channel centreline with wavelength $\lambda_z \approx 3h$, in the case of pure Couette flow. Therefore, to use the same definition for all the flow cases, we conventionally set the reference point for the conditional eddy analysis at the peak of the pre-multiplied energy spectrum for $\lambda_z = 3h$. The peaks thus determined are shown by crosses in figure 16. The occurrence of low-speed streaks is determined by chasing events characterized by intense negative streamwise velocity fluctuations, i.e. with $u'/u_{rms} < -1.5$. The conditionally sampled

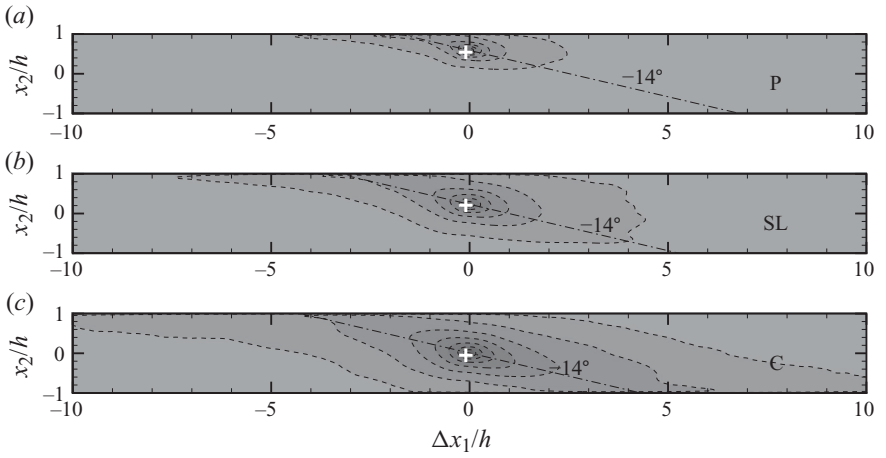

FIGURE 20. (*a–c*) Conditional expected fields associated with low-speed streaks ($u'/u_{rms} < -1.5$) at the outer low-wavenumber energy site (marked by a cross; see figure 16 for reference). Sixteen contour levels of u' are shown, $-0.13 \leqslant u'/u_p \leqslant 0.13$, the dashed lines denoting negative values. Note that only a limited streamwise portion of the computational domain is shown.

streamwise velocity and vorticity fields exhibit the typical organization of all shear flows (Hamilton *et al.* 1995), whose building blocks are momentum streaks flanked by pairs of counter-rotating quasi-streamwise vortices (rollers), which carry positive velocity fluctuations from regions of high momentum to regions of low momentum and vice versa. As recalled in the Introduction, streaks and streamwise vortices are at the heart of the currently accepted model of the turbulence regeneration mechanism in the presence of shear (Jiménez & Pinelli 1999; Schoppa & Hussain 2002).

For all flow cases, large-scale streaks are found to have a roughly circular core in the cross-stream plane, whose typical radius becomes of the order of the channel height in the case of the C flow. As can be inferred looking at the secondary minima in figure 19, the typical spanwise separation between streaks of the same sign may be up to $3h$. More important yet, the conditional fields associated with outer-layer streaks appear to extend to the nearest wall (and also to the opposite wall, as in the case of C flow), inducing the formation of oppositely signed vorticity owing to the no-slip condition. This scenario closely recalls the wall cycle mechanism of turbulence regeneration proposed by Orlandi & Jiménez (1994), whereby secondary vorticity is generated at solid walls from existing vortices because of the no-slip condition.

The projection of the conditional eddies in the x_1–x_2 plane, shown in figure 20, further illustrates the strong spatial coherence of the structures in the channel core, which extend for up to $20h$ and are inclined by about -14° with respect to the positive horizontal direction. Such an inclination (in absolute value) is very similar to that reported for the large-scale coherent structures in the logarithmic region of turbulent boundary layers (Marusic & Heuer 2007) and Poiseuille flows at high Reynolds number (Chung & McKeon 2010). We note that the negative sign of the inclination is due to the fact that the conditioning point in these examples lies in the upper part of the channel, where the mean shear is always negative (recalling figure 2). Placing the conditioning probe in regions with positive mean shear would yield the commonly quoted result that the inclination is $+14^\circ$.

5.3. *Amplitude modulation mechanism*

The possible occurrence of a modulating action of the large-scale outer motions in the small-scale near-wall structures was first investigated in the context of turbulent boundary-layer flow by Mathis *et al.* (2009*a*). They found that, in addition to the (linear) imprinting mechanism previously discussed, nonlinear phenomena of amplitude modulation (AM) also take place between the inner- and outer-layer eddies. They quantified the intensity of the amplitude modulation imparted by a large-scale eddy placed at a location P_1 on a small-scale eddy placed at another location P_2 by (i) determining the high-pass-filtered component of the velocity signal at P_2 (say, u_{2H}), (ii) determining the envelope of u_{2H} (say, u_{2E}) by means of the Hilbert transform, (iii) determining the low-pass-filtered component of the signal envelope (say, u_{2EL}) and (iv) calculating the correlation coefficient (hereafter referred to as amplitude modulation coefficient, R_{AM}) between the low-pass-filtered envelope at P_2 and the low-pass-filtered signal at P_1,

$$R_{AM}^{12} = \frac{\overline{u_{1L}\, u_{2EL}}}{\sqrt{\overline{u_{1L}^2}}\,\sqrt{\overline{u_{2EL}^2}}}. \tag{5.1}$$

Although the correlation can in general be applied to signals taken from two distinct points, Mathis *et al.* (2009*a*) argued that the one-point AM coefficient provides a reasonable estimate for the full two-point AM coefficient, and exploited a one-point analysis to quantify inner/outer interaction effects across the boundary layer. High levels of positive and negative correlation were observed in the inner and outer regions of the wall layer, respectively, with a zero crossing in the logarithmic region. According to the interpretation of Mathis *et al.* (2009*a*), the positive correlation found in the near-wall region indicates that positive (negative) large-scale velocity excursions induce local enhancement (suppression) of the small-scale turbulent velocity fluctuations. The opposite effect is observed in the outer layer. The analysis was extended to pipe and channel flows by Mathis *et al.* (2009*b*), who observed approximate invariance of the one-point AM coefficient in the inner region when data are compared at a similar friction Reynolds number.

The computed one-point AM correlation coefficient $R_{AM}^{11}(x_2)$ (for obvious reasons related to homogeneity of the flow, only the x_2 dependence is left) for C–P flows is reported in figure 21(*a*) as a function of the wall-normal outer-scaled coordinate. Note that, for the purpose of evaluating the various terms in (5.1), filtering is performed in the spanwise direction, with cutoff wavelength $\lambda_z = h$, which, based on the previous discussion, approximately marks the boundary between the small- and large-scale domains. The effect of varying the filter width was also addressed, but no qualitative change was observed. A trend consistent with the experiments of Mathis *et al.* (2009*b*) is found away from the wall when outer scaling is used, and in the near-wall region when inner scaling is used. Also accounting for the wide disparity in the Reynolds numbers and the different approaches used for filtering (spatial filtering is used here as opposed to filtering in the time domain), this makes us confident that the AM quantification procedure is properly implemented. Looking at the stationary wall, the typical behaviour observed in canonical wall-bounded flows is recovered for all the flow cases, with inversion of the sign of the modulation coefficient from positive to negative taking place just outside the buffer layer.

As shown by Schlatter & Örlü (2010), the one-point AM coefficient is strongly related to the local skewness of velocity fluctuations. Indeed, the streamwise velocity skewness, reported in figure 21(*b*), highlights remarkable similarities to the data

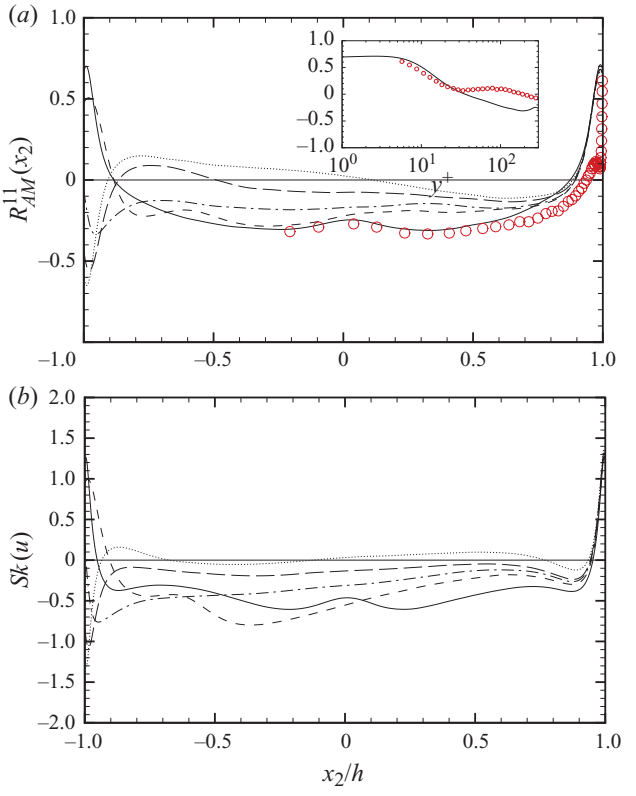

FIGURE 21. (Colour online) Distribution of (*a*) one-point amplitude modulation coefficient (R^{11}_{AM}), according to (5.1), and (*b*) skewness of streamwise velocity fluctuations. The symbols in (*a*) denote experimental data for the P flow at $Re_\tau = 3000$ (Mathis *et al.* 2009*b*). The inset in (*a*) shows a comparison between P flow data and experiments in semi-logarithmic representation. Lines: ——, P; – – –, P1; · – · –, SL; — —, C1; · · · ·, C.

reported in figure 21(*a*), especially near the wall. Incidentally, the skewness at the channel centreline is found to be negative for the P flow (as also found by Kim *et al.* 1987) and zero for the C flow (as found by Komminaho *et al.* 1996). Schlatter & Örlü (2010) were able to show that this similarity also persists when applying the AM analysis to synthetic random signals having the same probability density function as the original velocity signals (and thus non-zero skewness), indicating an inherent link between skewness and one-point modulation.

To overcome the possible limitations of the one-point modulation analysis, we propose fully exploiting the two-point AM correlation. Specifically, to evaluate the modulation mechanism we consider the two-point covariance between the large-scale velocity at P_1 and the low-pass-filtered envelope at P_2,

$$C^{12}_{AM} = \overline{u_{1L}\, u_{2EL}}. \tag{5.2}$$

The AM covariance is here preferred over the corresponding correlation coefficient, since it has the advantage of providing understanding of the absolute importance of the modulation effect between any two probe pairs. The modulation covariance thus defined is applied to the study of C–P class of flows by placing (as previously done for the conditional eddies) the conditioning point P_1 at a distance from the stationary wall corresponding to the peak of the spectral density for Fourier modes with $\lambda_z = 3h$,

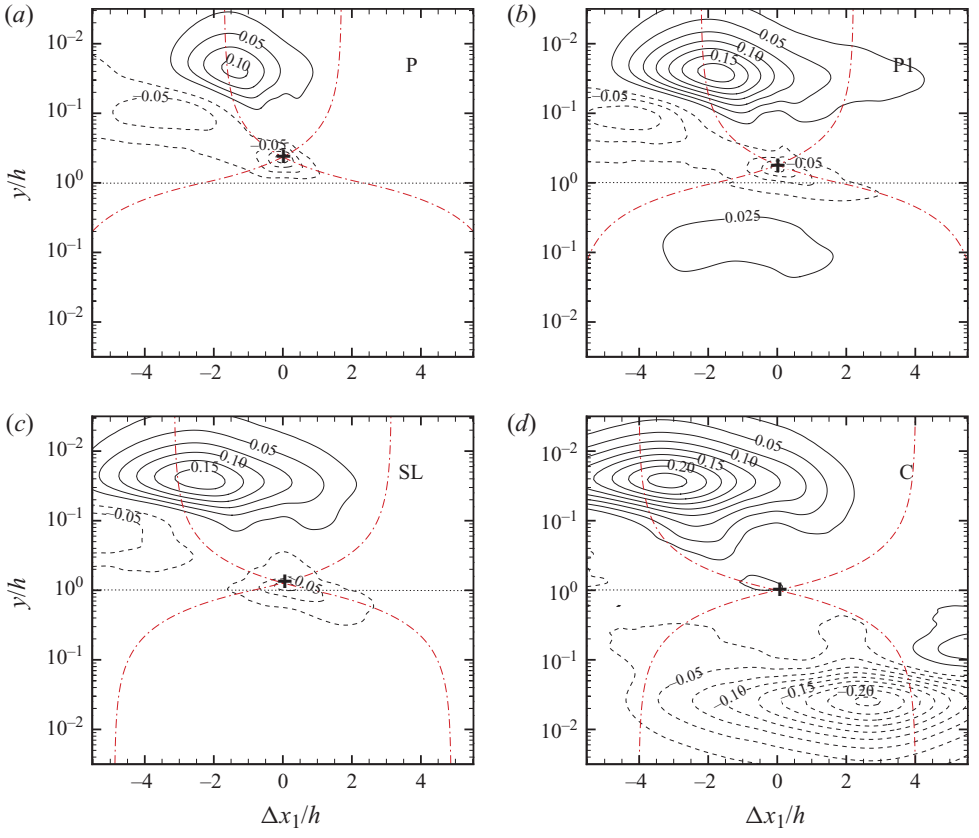

FIGURE 22. (Colour online) (*a–d*) Maps of the two-point AM covariance (C^{12}_{AM}), according to (5.2). The position of the modulating event is shown by a cross (see figure 16 for reference), and data are scaled with respect to $u^2_{\tau S}$. The dot-dashed lines indicate the local $\pm 14^\circ$ direction with respect to the horizontal direction.

which are representative of the large scales of motion. The probe P_2 is then displaced with respect to P_1 in the streamwise and wall-normal directions, thus obtaining AM covariance maps which depend on the wall-normal coordinate and the streamwise separation, say Δx_1.

The two-dimensional modulation maps obtained from this procedure are shown in figure 22. For clarity of the representation, the wall-normal distance (y) is reported (instead of x_2) in logarithmic scale to zoom into the near-wall region, and the position of the modulating probe is indicated by crosses. For guidance in the interpretation, the local $\pm 14^\circ$ directions about the modulating point are drawn with dot-dashed lines. In the case of the P flow, a scenario similar to that observed by Mathis *et al.* (2009*a*) is recovered, with a negative modulation peak around the conditioning point (associated with locally negative skewness) and a positive modulation peak located in the proximity of the nearby wall (in this case, the upper, stationary wall). Note that such a peak approximately leans in the same direction (-14°) with respect to the conditioning point as the conditional eddies shown in figure 20. The same qualitative scenario is also found for the P1 and the SL flows, for which the modulating influence on the near-wall region becomes stronger. In the case of the C flow, it is

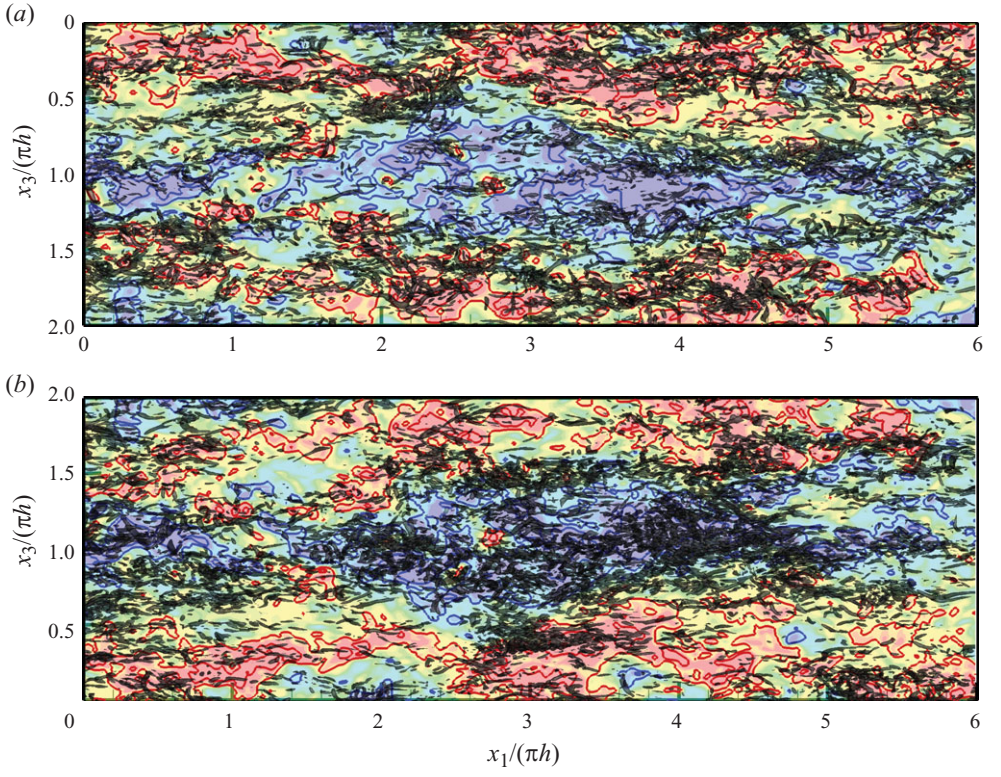

FIGURE 23. Coherent vortices near the (*a*) stationary and (*b*) moving wall for the C flow, educed as iso-surfaces of the swirling strength ($\lambda_{ci} = 1.25\,u_p/h$, black shades), superposed on flooded contours of u'/u_{rms} at the channel centreplane (the iso-lines -1, -2 are in blue and the iso-lines 1, 2 are in red). Only a quarter of the full domain is shown.

found that the centreline velocity has a modulating influence on both the moving and the stationary walls. In this case, the modulation covariance imparted on the stationary wall has positive sign, whereas negative modulation is observed at the moving wall. Also, in this case the modulation peaks lie along a line having small negative inclination with respect to the horizontal, even though the characteristic angle seems to be somewhat larger than 14° in absolute value. It is remarkable that the site where the peak modulation occurs lies, for all cases, at a wall distance $y^+ \approx 6.5$, and its influence extends to both the viscous sublayer and the buffer zone.

The patterns observed in figure 22(*c*) can be interpreted by noting that, in the case of the C-like flows, a positive large-scale velocity fluctuation near the centre of the channel causes the reduction of the velocity gradient at the moving wall (with subsequent reduction of the turbulent activity) and the increase of the wall friction at the stationary wall (with enhancement of the turbulent activity). Recalling figure 11(*c*), one can indeed observe a noticeable clustering of small-scale streaks near the moving wall corresponding to regions of local low momentum at the channel centreline, whereas the opposite effect is found near the stationary wall (see figure 9*c*). A clearer illustration of the modulation mechanism is obtained by superposing the velocity fields at the centreline with the small-scale vortical structures educed near the two walls, as shown in figure 23 for the C flow. Vortex cores have been extracted

using the criterion developed by Zhou *et al.* (1999), based on the imaginary part of the complex conjugate eigenvalue pair of the velocity gradient tensor (the so-called swirling strength, here referred to as λ_{ci}). The figure shows a remarkable association between low-momentum zones at the channel centreline (shown by blue contours) and zones of strong vortical activity near the moving wall, and zones depleted with vortices near the stationary wall. The opposite effect is observed for high-momentum zones at the channel centreline (shown by red contours) in figure 23.

An alternative strategy for quantifying inner/outer interactions in terms of modulating influences has recently been proposed by Guala, Metzger & McKeon (2011) in the study of the atmospheric surface layer, which apparently is not biased by non-zero skewness of the velocity signal. The implementation of that strategy could usefully complement the results of the present study.

6. Conclusions

The structure of turbulence in Couette–Poiseuille flows has been investigated by means of DNS. A series of flow conditions have been covered, including the limiting cases of pure Poiseuille flow (canonical channel flow), pure Couette flow and shear-less flow (near-zero shear at the moving wall). This class of flows is of particular interest since it allows study of the effect of changing the conditions at one of the walls (in this case, changing its velocity) on the opposing one. The study has the main merit of allowing insight into the effect of the large-scale channel dynamics on the structure of near-wall turbulence, even at the moderate Reynolds numbers considered.

The results indicate the absence of true large-scale dynamics for the P-like flows, which is associated with the lack of significant transport of turbulence kinetic energy from one wall to the other. In this case, the effect of one wall approximately extends up to the position where the maximum mean velocity is attained, and turbulence kinetic energy production vanishes. On the other hand, global influence of the moving wall on the entire flow is observed for C-like flows, associated with the establishment of large-scale motions in the channel core, whose typical length and width are of the order of $10h$ (at least) and $3h$, respectively. Such large-scale motions come in the form of low- and high-speed streaks associated with small (but non-zero) values of the shear near the middle of the channel, unlike the case for canonical channel and pipe flow.

The velocity statistics near both the stationary and the moving wall indicate lack of collapse in classical wall scaling, with a general tendency of turbulence intensities to increase from P to C flow, which is consistent with an increased imprinting of the large-scale motions on near-wall turbulence. Indeed, as well shown by the velocity spectra, the outer-scaled motions that form for C-like flows maintain a clear footprint in the near-wall region, providing additional energy at low wavenumbers. The large-scale motions are found to have much more 'isotropic' behaviour, since they perceive the constraining effect of the walls more weakly. As a consequence, it is found that the wall-parallel velocity components are more significantly affected by the wall motion than the streamwise velocity, whose peak is associated with the strongly anisotropic nature of the small-scale velocity fluctuations near the walls. The improved collapse of the velocity statistics in the core of the channel when local friction scaling is used suggests similarities with homogeneously sheared flows. However, differences persist between different flows, the r.m.s. velocity fluctuations varying in the range $8 \leqslant u_{rms}/u_{\tau L}(x_2) \leqslant 14$ (figure 7*a*).

The study of the geometry of the velocity field has shown that the formation/suppression of streaks is approximately controlled by the local turbulence kinetic

energy production/dissipation ratio, as proposed by Lam & Banerjee (1992), the streaks vanishing around local extrema of the mean velocity profile. In that case, the local geometry of the flow is found to be strongly affected by the blocking effect of the wall. The streak spacing is found to vary by almost an order of magnitude across the flow cases, when reported in classical wall scaling. Much better universality is found in the channel core when local scaling is used, in which case streak spacings in the range $50 \leqslant \lambda_z/\ell_L(x_2) \leqslant 100$ are obtained. This result again points not only to the validity of local viscous scaling in establishing the turbulence properties, but also to the need to incorporate (in some form) the pressure gradient in the analysis to achieve collapse of flow statistics among different flow cases (Johnstone *et al.* 2010).

The analysis of the effect of the large-scale structures which form in the channel core on the turbulence dynamics near the two walls has highlighted the occurrence of a more subtle influence than simple imprinting, which is very similar to the amplitude modulation mechanisms observed in high-Reynolds-number boundary layers and channels. In first instance, visualizations of C-like flows clearly indicate that the low-momentum regions found near the channel centreline are associated with regions of increased turbulent activity near the moving wall. This modulating effect has been characterized through an extension of the procedure developed by Mathis *et al.* (2009*a*), and based on the design of a two-point amplitude modulation covariance. This tool allows inference of a growing near-wall influence of the outer-layer structures in the case of C-like flows. In this case, the modulating influence near the stationary wall manifests itself with the appearance of a positive lobe of the amplitude modulation covariance at a wall distance $y^+ \approx 6.5$, which is primarily caused by local decrease of the wall friction induced by large-scale low-momentum deficit at the channel centre. The opposite effect is observed near the stationary wall. Secondly, the analysis of the conditional average coherent structures in the channel core shows the emergence (at least in statistical sense) of large momentum streaks associated with pairs of quasi-streamwise vortices, which promote the formation of secondary near-wall streamwise vorticity because of the no-slip condition. The latter effect is reminiscent of the wall cycle of turbulence self-sustainment envisaged by Orlandi & Jiménez (1994). Jiménez & Pinelli (1999) provided hints that in the case of canonical channel flows this mechanism has less dynamical significance than the primary streaks regeneration mechanism. It would then be interesting to verify whether the same conclusions also apply to Poiseuille flow, in which case, based on the results reported in this paper, greater relevance of the wall cycle seems possible.

In perspective, we believe that the class of C–P flows can be conveniently utilized to analyse in a simple setting some mechanisms of wall-bounded flows, such as the formation of large structures and the inner–outer interactions, which (so far) have only been observed in experiments and DNS at large Reynolds numbers. Of special importance may be the case of the shear-less flow, which does not seem to have been thoroughly studied so far, and which is of interest for the analysis of wall turbulence near a separation point. Much interest may also reside in the analysis of the large- and small-scale contributions to the Reynolds shear stress, which is the turbulence statistics of primary importance. In this respect, this study seems to suggest universality of the contribution of the small scales, which, if confirmed for other Reynolds numbers and/or flow cases, would be of extreme theoretical interest. We also expect that the database reported in the present paper can be of use for a RANS modeller, providing access to statistics for wall-bounded flows in the presence of non-zero pressure gradients (Borello & Orlandi 2011).

This research was started and partially supported by the Sixth Framework Programme European project WALLTURB. The authors acknowledge the CASPUR supercomputing consortium for providing the resources to perform the numerical simulations.

REFERENCES

del Álamo, J. C. & Jiménez, J. 2009 Estimation of turbulent convection velocities and corrections to Taylor's approximation. *J. Fluid Mech.* **640**, 5–26.

Bech, K. H., Tillmark, N., Alfredsson, P. H. & Andersson, H. I. 1995 An investigation of turbulent plane Couette flow at low Reynolds numbers. *J. Fluid Mech.* **286**, 291–325.

Borello, D. & Orlandi, P. 2011 DNS scrutiny of the $z-f$ elliptic-relaxation eddy-viscosity model in channel flows with a moving wall. *Flow Turbul. Combust.* **86**, 295–300.

Chung, D. & McKeon, B. K. 2010 Large-eddy simulation of large-scale structures in long channel flow. *J. Fluid Mech.* **661**, 341–364.

El Telbany, M. M. M. & Reynolds, A. J. 1980 Velocity distributions in plane turbulent channel flows. *J. Fluid Mech.* **100**, 1–29.

El Telbany, M. M. M. & Reynolds, A. J. 1981 Turbulence in plane channel flows. *J. Fluid Mech.* **111**, 283–318.

Guala, M., Metzger, M. & McKeon, B. J. 2011 Interactions within the turbulent boundary layer at high Reynolds number. *J. Fluid Mech.* **666**, 573–604.

Hamilton, J. M., Kim, J. & Waleffe, F. 1995 Regeneration mechanisms of near-wall turbulent structures. *J. Fluid Mech.* **287**, 317–348.

Hoyas, S. & Jiménez, J. 2006 Scaling of velocity fluctuations in turbulent channels up to $Re_\tau = 2003$. *Phys. Fluids* **18**, 011702.

Hutchins, N. & Marusic, I. 2007 Large-scale influences in near-wall turbulence. *Phil. Trans. R. Soc. Lond.* A **365**, 647–664.

Jiménez, J., Hoyas, S., Simens, M. P. & Mizuno, Y. 2010 Turbulent boundary layers and channels at moderate Reynolds numbers. *J. Fluid Mech.* **657**, 336–360.

Jiménez, J. & Pinelli, A. 1999 The autonomous cycle of near–wall turbulence. *J. Fluid Mech.* **389**, 335–359.

Johnstone, R., Coleman, G. N. & Spalart, P. R. 2010 The resilience of the logarithmic law to pressure gradients: evidence from direct numerical simulation. *J. Fluid Mech.* **643**, 163–175.

Kim, J., Moin, P. & Moser, R. 1987 Turbulence statistics in fully developed channel flow at low Reynolds number. *J. Fluid Mech.* **177**, 133–166.

Kim, K. C. & Adrian, R. J. 1999 Very large-scale motion in the outer layer. *Phys. Fluids* **11**, 417–422.

Kitoh, O., Nakabayashi, K. & Nishimura, F. 2005 Experimental study on mean velocity and turbulence characteristics of plane Couette flow: low-Reynolds-number effects and large longitudinal vortical structure. *J. Fluid Mech.* **539**, 199–227.

Klebanoff, P. S. 1955 Characteristics of turbulence in a boundary layer with zero pressure gradient. *NACA Rep.* 1247.

Kline, S. J., Reynolds, W. C., Schraub, W. C. & Runstadler, F. A. 1967 The structure of turbulent boundary layers. *J. Fluid Mech.* **30**, 741–773.

Komminaho, J., Lundbladh, A. & Johansson, A. V. 1996 Very large structures in plane turbulent Couette flow. *J. Fluid Mech.* **320**, 259–285.

Kuroda, A., Kasagi, N. & Hirata, M. 1993 Direct numerical simulation of turbulent plane Couette–Poiseuille flows: effect of mean shear on the near-wall turbulence structures. In *Proc. 9th Symp. Turbulent Shear Flows, Kyoto*, vol. 1, pp. 8.4.1–8.4.6.

Lam, K. & Banerjee, S. 1992 On the condition of streak formation in a bounded turbulent flow. *Phys. Fluids* **4**, 306–320.

Lee, M. L., Kim, J. & Moin, P. 1990 Structure of turbulence at high shear rate. *J. Fluid Mech.* **216**, 561–583.

Marusic, I. & Heuer, W. D. C. 2007 Reynolds number invariance of the structure inclination angle in wall turbulence. *Phys. Rev. Lett.* **99**, 114504.

Marusic, I., Mathis, R. & Hutchins, N. 2010 High Reynolds number effects in wall turbulence. *Intl J. Heat Fluid Flow* **31**, 418–428.

Mathis, R., Hutchins, N. & Marusic, I. 2009*a* Large-scale amplitude modulation of the small-scale structures in turbulent boundary layers. *J. Fluid Mech.* **628**, 311–337.

Mathis, R., Monty, J. P., Hutchins, N. & Marusic, I. 2009*b* Comparison of large-scale amplitude modulation in turbulent boundary layers, pipes, and channel flows. *Phys. Fluids* **21**, 111703.

Monty, J., Hutchins, N., Ng, H. C. H., Marusic, I. & Chong, M. S. 2009 A comparison of turbulent pipe, channel and boundary layer flows. *J. Fluid Mech.* **632**, 431–442.

Monty, J. P., Stewart, J. A., Williams, R. C. & Chong, M. S. 2007 Large-scale features in turbulent pipe and channel flows. *J. Fluid Mech.* **589**, 147–156.

Morrison, J. F. 2007 The interaction between inner and outer regions of turbulent wall-bounded flow. *Phil. Trans. R. Soc. Lond.* A **365**, 683–698.

Nakabayashi, K., Kitoh, O. & Katoh, Y. 2004 Similarity laws of velocity profiles and turbulence characteristics of Couette–Poiseuille turbulent flows. *J. Fluid Mech.* **507**, 43–69.

Orlandi, P. 2000 *Fluid Flow Phenomena: A Numerical Toolkit*. Kluwer.

Orlandi, P. & Jiménez, J. 1994 On the generation of turbulent wall friction. *Phys. Fluids* **6**, 634–641.

Robinson, S. K. 1991 Coherent motions in the turbulent boundary layer. *Annu. Rev. Fluid Mech.* **23**, 601–639.

Schlatter, P. & Örlü, R. 2010 Quantifying the interaction between large and small scales in wall-bounded turbulent flows: a note of caution. *Phys. Fluids* **22**, 051704.

Schlatter, P., Örlü, R., Li, Q., Brethouwer, G., Fransson, J. H. M., Johansson, A. V., Alfredsson, P. H. & Henningson, D. S. 2009 Turbulent boundary layers up to $Re_\theta = 2500$ studied through simulation and experiment. *Phys. Fluids* **21**, 051702.

Schlichting, H. & Gersten, K. 2000 *Boundary Layer Theory*, 8th edn. Springer.

Schoppa, W. & Hussain, F. 2002 Coherent structure generation in near-wall turbulence. *J. Fluid Mech.* **453**, 57–108.

Smith, R. & Metzler, P. 1983 The characteristics of low-speed streaks in the near-wall region of a turbulent boundary layer. *J. Fluid Mech.* **129**, 27–54.

Spencer, N. B., Lee, L. L., Parthasarathy, R. N. & Papavassiliou, D. V. 2009 Turbulence structure for plane Pouiseuille–Couette flow and implications for drag reduction over surfaces with slip. *Can. J. Chem.* **87**, 38–46.

Thurlow, E. M. & Klewicki, J. C. 2000 Experimental study of turbulent Poiseuille–Couette flow. *Phys. Fluids* **12**, 865–875.

Townsend, A. A. 1976 *The Structure of Turbulent Shear Flow*, 2nd edn. Cambridge University Press.

Wallace, J. M., Eckelmann, H. & Brodkey, R. S. 1972 The wall region in turbulent shear flow. *J. Fluid Mech.* **54**, 39–48.

Willmarth, W. W. & Lu, S. S. 1972 Structure of the Reynolds stress near the wall. *J. Fluid Mech.* **55**, 65–92.

Zhou, J., Adrian, R. J., Balachandar, S. & Kendall, T. M. 1999 Mechanisms for generating coherent packets of hairpin vortices in channel flow. *J. Fluid Mech.* **387**, 353–396.